Synthesis and Characterization of an Ionomer for Zinc-Air Battery Cathodes

by

Manuel Padilla

A Thesis Presented in Partial Fulfillment
of the Requirements for the Degree
Master of Science

Approved November 2012 by the
Graduate Supervisory Committee:

Cody Friesen, Chair
Daniel Buttry
Karl Sieradzki

ARIZONA STATE UNIVERSITY

December 2012

ABSTRACT

The work presented in this thesis covers the synthesis and characterization of an ionomer that is applicable to zinc-air batteries. Polysulfone polymer is first chloromethylated and then quaternized to create an ion-conducting polymer. Nuclear magnetic resonance (NMR) spectra indicates that the degree of chloromethylation was 114%. The chemical and physical properties that were investigated include: the ionic conductivity, ion exchange capacity, water retention capacity, diameter and thickness swelling ratios, porosity, glass transition temperature, ionic conductivity enhanced by free salt addition, and the concentration and diffusivity of oxygen within the ionomer. It was found that the fully hydrated hydroxide form of the ionomer had a room temperature ionic conductivity of 39.92mS/cm while the chloride form had a room temperature ionic conductivity of 11.80mS/cm. The ion exchange capacity of the ionomer was found to be 1.022mmol/g. The water retention capacity (WRC) of the hydroxide form was found to be 172.6% while the chloride form had a WRC of 67.9%. The hydroxide form of the ionomer had a diameter swelling ratio of 34% and a thickness swelling ratio of 55%. The chloride form had a diameter swelling ratio of 32% and a thickness swelling ratio of 28%. The largest pore size in the ionomer was found to be 32.6nm in diameter. The glass transition temperature of the ionomer is speculated to be 344°C. A definite measurement could not be made. The room temperature ionic conductivity at 50% relative humidity was improved to 12.90mS/cm with the addition of 80% free salt. The concentration and diffusivity of oxygen in the ionomer was found to be 1.3 ±0.2mMol and (0.49 ±0.15)x10^{-5} cm^2/s respectively. The ionomer synthesized in this research had material properties and performance that is comparable to other ionomers

reported in the literature. This is an indication that this ionomer is suitable for further study and integration into a zinc-air battery. This thesis is concluded with suggestions for future research that is focused on improving the performance of the ionomer as well as improving the methodology.

DEDICATION

I would like to dedicate this research to both of my parents, Dr. Jose Manuel Padilla Mora and Marcela Padilla Garcia Herrera. I dedicate this work to my father because of all the wisdom, guidance, and advice he gave me throughout my college and graduate school career. I dedicate this work to my mother because of her inexhaustible and unconditional love and support. It is indubitable that this work would not have been completed without them. I further dedicate this work to both of my brothers, Diego and Andres Padilla, for being the best friends a man could ask for. Life would not be the same without my brothers. Lastly, I want to include the rest of my family and friends in this dedication for their continued support and encouragement throughout my graduate school career. I am truly a fortunate man to have a great family and many great friends.

ACKNOWLEDGMENTS

I want to thank my graduate advisor, Dr. Cody A. Friesen, for his mentorship and guidance throughout my graduate school experience. I want to especially thank him for providing me with an incredible opportunity to expand my knowledge of cutting edge technology and science. I consider myself very fortunate to have Dr. Friesen as my advisor and I truly enjoyed working for him.

I would like to also thank Fluidic Energy and ARPA-E for funding my research and providing me with top of the line equipment. My research experience with Fluidic Energy was very rewarding. In addition, I would like to thank various members of the Fluidic Energy team for their assistance in my research. I thank Dr. Lei “Toni” Tang for her expertise in electrochemistry and the guidance she gave me in conducting experiments; Carl Neuburger for his expertise in materials processing; Dr. Robert “Bob” Zeller for his expertise in electrochemistry and materials science; Paul B. Johnson for his expertise in materials science; Dr. Elise Switzer for her expertise in electrochemistry, and Dr. Derek Wolfe for his expertise in synthetic chemistry. These people form a truly talented team of professionals that gave me access to a wealth of knowledge and skill sets; I consider myself very fortunate for having the opportunity to learn from and work with this talented team. Lastly, I would also like to acknowledge Audrey Willman, Kristi Hofheins, and Boris Puzhaev for their encouragement and support.

Many thanks go to various individuals at Arizona State University that made my research possible. I deeply thank Dr. Terry Alford and Yolanda Murphy for their mentoring, advice, and nominating me for the Reach for the Stars Fellowship. I would like to thank the Graduate College and all of the people who

made the Reach for the Stars Fellowship possible; this fellowship provided me with generous financial support that is superlatively appreciated. I thank Dr. Brian Cherry and the Magnetic Resonance Research Center at Arizona State University for his help with testing NMR samples. I thank Kirk Vance for his help with the DSC measurements. Lastly, I would like to thank all of my professors in both my undergraduate and graduate careers for providing me with a truly exceptional tier 1 education.

TABLE OF CONTENTS

Page

CHAPTER Page

LIST OF TABLES

LIST OF FIGURES

CHAPTER 1

INTRODUCTION

1.1 Motivational Introduction

Energy production and storage has always been a highly studied topic since the dawn of mankind. This is especially true today now that the issue of diminishing fossil fuel sources and their negative impact on the environment continues to receive more attention in the media. There is no doubt that an energy storage solution that can compete with fossil fuels in terms of energy density is highly desired by most societies. In addition to improved energy density, safety and environmental friendliness must also be a consideration factored into the solution. The chemical battery can be one such solution and is arguably the most studied energy storage technology. Currently, the lithium-ion battery remains as one of the highest performing commercially available batteries.

The lithium ion battery is found in most high tech devices today including portable computers such as laptops and touch pads, cell phones, music players, and other mobile devices. These batteries are optimized to meet the demands of a specific application. For example, mobile electronic devices will require a battery that is compact yet offer a large enough energy density to power the device for hours of continuous use. Other applications, such as radio controlled airplanes and model cars, require a light weight lithium ion battery that can provide high discharge rates and power densities. Lithium polymer batteries are popular for those kinds of applications. There are numerous other applications that benefit from the use of lithium ion batteries. In fact, the lithium ion battery business has grown to become a multibillion dollar global industry [3]. Most of

these lithium ion batteries on the market today use a graphitic carbon anode, an organic liquid solvent electrolyte that contains dissolved lithium salts, and a lithium-intercalated transition-metal oxide cathode [3]. While these cells are primarily the norm in portable electronic device industries, they have not been able to gain the same foothold in the transportation industry. There are many challenges that must be overcome before they can become a feasible replacement for current internal combustion engine vehicles.

One obvious challenge is that the energy density of these batteries has yet to match that of liquid fuels. Liquid fuels can store more energy per unit volume than any commercially available lithium ion battery. This means that an arbitrary fixed volume of a liquid fuel such as gasoline can drive a vehicle farther than a battery of equal volume can, holding everything else constant. Another challenge is that the power density of lithium ion batteries cannot match that of liquid fuels either. Liquid fuels can be combusted to release its energy almost instantaneously. In contrast, lithium ion batteries are severely limited by how fast they can discharge their stored energy. It is suffice to say that the performance of lithium ion batteries has yet to even come close to that of liquid fuels. This will be a major holdback for electric vehicles until battery performance can be improved upon.

Another drawback to lithium ion batteries is that their safety and reliability remains to be a major concern. Lithium ion batteries have been recalled for safety issues in the past due to dangerous failures [3]. These batteries are known to rupture, ignite, and even explode when exposed to high temperatures. Additionally, short circuiting a lithium ion battery can also cause a devastating malfunction. Lithium polymer batteries are very susceptible to rupturing and

starting fires if they are over-charged. For example, it is typically recommended that RC-hobby lithium polymer batteries be charged within a fireproof bag for added safety. The major safety issue in these batteries is the use of a liquid electrolyte and a very reactive transition-metal oxide electrode [3].

So even though lithium ion and lithium polymer batteries seem like a promising solution to powering larger electrical applications, one can easily see that some issues need be addressed before they completely replace gasoline as a fuel source. There are currently a few battery powered electric vehicles available in the automotive market such as the Tesla Model S, Ford Focus Electric, Chevrolet Volt, Nissan LEAF, and Toyota RAV4 EV to name a few. However, these vehicles typically have a limited driving range which averages around 100 miles on a full battery charge. For the most part, these current electric vehicles are limited to short range city driving and will require daily charging. Long range road trips are very difficult to accomplish since interstate charging stations are still scarce. The future battery that powers electric vehicles, and other large scale electrical devices, will need to be robust to high temperatures, environmentally safe in case of a mechanical failure, offer the required power and energy densities, and be relatively affordable. One such technology that is being studied extensively, and might fit the bill, is the metal-air battery. The reader should note that the work presented in this thesis is specifically about the synthesis and characterizing an ion-conducting polymer that is compatible with the air-cathodes of metal-air batteries. However, a brief discussion of metal-air batteries, and more specifically zinc-air batteries, is presented for the reader's own benefit.

1.2 Introduction to Metal-Air Batteries

One of the more promising battery technologies being developed today are metal-air batteries. Metal-air batteries typically have a solid metal anode such as lithium, aluminum, zinc, sodium, calcium, and beryllium to name a few. The electrolyte in commercially available primary metal-air batteries, such as zinc-air, is usually an alkaline aqueous solution or gel. More specifically, potassium or sodium hydroxide based electrolytes are used. The cathode is actually molecular oxygen, which gets reduced on a high surface area carbon-based structure. The reader should note that the structure that reduces oxygen is also referred to as an air-cathode or simply the cathode. Details of these components will be further discussed in the pages that follow. These batteries are referred to as metal-air batteries since they are able to use the required oxygen from the air in which they will operate. This gives the battery the advantage of not needing to store one of its chemical reagents within its own structure since the air-cathodes are breathable. Because of this particular advantage, the theoretical energy densities for metal-air batteries are encouragingly high.

Table 1 below is a comparison of several highly studied metal-air batteries [84].

Table 1. Characteristic parameters of popular metal-air batteries.

Metal anode	Electrochemical equivalent of metal, Ah/g	Theoretical cell voltage,* V	Valence change	Theoretical specific energy (of metal), kWh/kg	Practical operating voltage, V
Li	3.86	3.4	1	13.0	2.4
Ca	1.34	3.4	2	4.6	2.0
Mg	2.20	3.1	2	6.8	1.2–1.4
Al	2.98	2.7	3	8.1	1.1–1.4
Zn	0.82	1.6	2	1.3	1.0–1.2
Fe	0.96	1.3	2	1.2	1.0

* Cell voltage with oxygen cathode.

It can be seen from table 1 that the lithium metal anode has the highest electrochemical equivalency per gram and is one of the primary reasons why lithium ion batteries generate so much interest. This advantage is further reflected in the theoretical specific energy of the lithium-air battery cell. Couple that with a high cell voltage and it becomes obvious why lithium-air batteries are highly researched. Figure 1 below compares the theoretical specific energy of the lithium-air and zinc-air battery cells to that of current technologies [86].

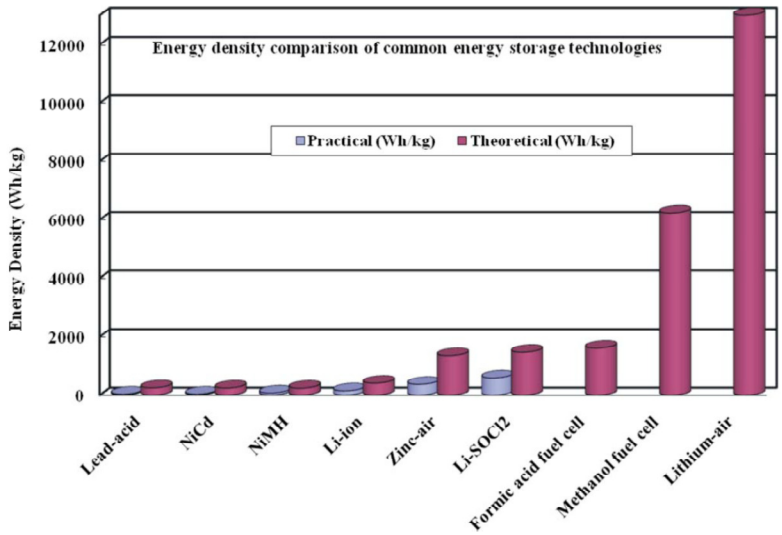

Figure 1. Energy density comparison for various common battery and fuel cell technologies.

It should be noted that the energy densities reported for the fuel cells in figure 1 are based solely on the energy content of the fuel and do not take into consideration the mass of the actual power plant. Accounting for the actual hardware of the fuel cell will lower its theoretical energy density. Nevertheless, it can be seen that the lithium-air battery system has a theoretical energy density that is much higher than its competition. The zinc-air battery system achieves the

second highest practical energy density beating out the lithium ion battery system and being beaten only by the lithium thionyl chloride battery system. It's easy to see why metal-air batteries have garnered so much interest.

Metal-air batteries have some distinct advantages that other battery systems do not. For example, in addition to high energy densities, these batteries also typically have flat discharge voltages, they have very long shelf lives when properly sealed, they present little or no ecological problems, the cost of the batteries is low if based on the use of metals, and the capacity of the battery is typically independent of load and temperature when operating within its normal range of operation [84]. However, these batteries are not without their flaws either. Some typical drawbacks to metal-air batteries include: the shelf life maybe significantly reduced if the electrolyte dries out, flooding of the electrolyte may limit power output, limited operating temperature range, carbonation of the alkali electrolyte, molecular hydrogen maybe produced from the corrosion of the anode, and lastly, metal-air batteries typically have lower power densities by comparison to other energy storage technologies [84].

1.3 Introduction to Zinc-Air Batteries

The work presented in this thesis is applicable to almost any metal-air battery, but has been tailored specifically for the zinc-air battery system. The zinc-air battery system by itself offers distinct advantages over the other metal-air battery systems. Firstly, zinc is a low cost metal that is readily available; it is the 24^{th} most abundant element in the Earth's crust and the largest ore deposits are located in Asia, Australia, and the United States. Secondly, unlike lithium metal, zinc has very low reactivity making it a great candidate for an environmentally safe product. Electrochemical advantages include the high electropositivity of

zinc metal which makes it stable in aqueous and alkaline electrolytes without significant corrosion provided that appropriate inhibitors are used [84]. Furthermore, zinc is the most active metal that can be electrodeposited from an aqueous electrolyte making it highly favorable for secondary batteries [84]. However, some drawbacks specific to zinc metal include: problems with dendrite formation, limited solubility of the reaction product, and non-uniform zinc deposition and dissolution. The researcher believes that the benefits of using zinc metal heavily outweigh the drawbacks, and thus this research is focused on contributing to the improvement of the zinc-air battery system. However, before the core aspects of this research are detailed, a brief explanation of the zinc-air chemistry will be given in the paragraphs that follow.

As stated previously, the anode reactant is zinc metal while the cathode reactant is molecular oxygen. Since the metal-air battery is exposed to air, it can be assumed that the supply of oxygen is limitless. Therefore, increasing the capacity of the cell only requires increasing the amount of zinc present. The air-cathode present in a zinc-air battery serves only to reduce oxygen during discharge of the cell and itself is not consumed in the reaction. In theory, the air-cathode has an infinite service life and its electrochemical properties remain unchanged during cell discharge. Its physical size does not change either.

There are numerous methods for manufacturing air-cathodes; however they all have a few things in common. Air-cathodes must be porous to allow for the diffusion of oxygen to the electrolyte boundary and incorporate a material where oxygen can be reduced. Typically, high surface area carbon black is used for this purpose. Since carbon black comes in a powder form, a binder is usually needed to hold the carbon black together and provide structural integrity. There

are many choices for binders; DuPont Teflon polytetrafluoroethylene (PTFE) is a popular choice [87]. In addition, a catalyst such as platinum may be added to the mixture of carbon black and binder to further improve current densities. These materials are usually solution processed and then hot pressed onto a current collector such as a nickel mesh or foam that will further improve the structural integrity of the electrode and collect the charge that is passed. Using nickel mesh offers the advantage that in addition to serving as a current collector, nickel metal is also a great catalyst for the oxygen reduction reaction. The end result is a structure that is compact yet porous and electrochemically active.

The reactions that occur at the cathode are actually quite complex; however, they can be simplified to the following [85]:

$Reaction\ 1$: $$O_2 + 2H_2O + 4e^- \rightarrow 4OH^-$$

Reaction 1 has a standard potential of 0.4V [85]. There is actually a rate limiting step in reaction 1. This rate limiting step affects the kinetics of the chemical reaction and thus the performance of the battery. A peroxide free radical is formed during the reaction presented above which must be decomposed [85].

$Step\ 1$: $$2O_2 + 2H_2O + 4e^- \rightarrow 2O_2H^- + 2OH^-$$

$Step\ 2$: $$2O_2H^- \rightarrow O_2 + 2OH^-$$

Adding steps 1 and 2 together will yield the overall reaction, i.e. reaction 1. The actual rate limiting step is the decomposition of the peroxide free radical to the hydroxide anion, i.e. step 2. Since this step limits the overall reaction kinetics of reaction 1, it is important to catalyze it so that battery performance can be maximized. Air-cathodes typically have built in catalysts that promote step 2 in the formation/decomposition of the peroxide free radical. These catalysts include elemental silver and nickel, noble metals such as platinum and their compounds,

cobalt oxide, manganese dioxide, mixed metal compounds including rare earth metals and transition metal macrocyclics, spinels, and phtalocyanines or perovskites [85].

At the anode, elemental zinc is oxidized and reacted to form the zincate anion as the discharge product. The reaction can be seen below:

$Reaction\ 2$: $2Zn + 8OH^- \rightarrow 2Zn(OH)_4^{-2} + 4e^-$

Reaction 2 has a standard potential of 1.25V [85]. Reaction 2 proceeds until the local environment becomes saturated with the zincate anion. At this point, the zincate anion decomposes to precipitate zinc oxide [85].

$Reaction\ 3$: $2Zn(OH)_4^{-2} \rightarrow 2ZnO + 2H_2O + 4OH^-$

Adding reactions 1, 2, and 3 yields the overall cell reaction in the zinc-air battery.

$Reaction\ 1$: $O_2 + 2H_2O + 4e^- \rightarrow 4OH^-$ $E° = 0.4V$

$Reaction\ 2$: $2Zn + 8OH^- \rightarrow 2Zn(OH)_4^{-2} + 4e^-$ $E° = 1.25V$

$Reaction\ 3$: $2Zn(OH)_4^{-2} \rightarrow 2ZnO + 2H_2O + 4OH^-$

$Overall$: $O_2 + 2Zn \rightarrow 2ZnO$ $E° = 1.65V$

The above overall reaction has a standard potential of 1.65V and is the maximum theoretical potential a zinc-air battery can have. Real zinc-air cells will most likely have a cell potential less than the theoretical limit.

Zinc-air batteries typically have an aqueous or gel, alkaline electrolyte. In fact, the ion-conducting polymer studied in this work is indeed alkaline. This polymer, which is commonly known as an ionomer, is integrated with the air-cathode and is responsible for transporting the hydroxide anions that are generated in reaction 1. The ionomer, which serves as part of an electrolyte system, will then need to be chemically coupled to a secondary electrolyte which will be responsible for transporting the ions created in reactions 2 and 3. This

secondary electrolyte can be an aqueous solution, an ionic liquid, or even a different solid material capable of transporting the necessary ions. However, the reader should note that this thesis is based solely on the study of the ionomer that is coupled to the air-cathode in a zinc-air battery. As such, all experiments presented here will be closely related to the compounds in reaction 1. Study of the secondary electrolyte, which is coupled to the zinc anode, is left for future research.

The use of an ionomer in a zinc-air battery has many motivations. First an ionomer can assist in slowing down, or even eliminating, the evaporation of water in a zinc-air battery. Being able to reduce or eliminate water loss from the electrolyte in the cell will definitely prolong the shelf life of a metal-air battery. In addition, using a thin ionomer membrane could allow for the manufacture of very thin zinc-air battery cells. Having thin cells with large energy densities will be of utmost importance to the consumer electronics industry since technology companies are constantly pushing for thinner and lighter weight devices. Lastly, ionomer membranes can help make zinc-air batteries safer for the environment. The membrane can serve as an electrolyte separator that prevents the secondary electrolyte from spilling out of the air cathode if the secondary electrolyte happens to be a hazardous liquid.

1.4 Overview of Thesis Work

The ionomer used in this work is a functionalized form of a polysulfone polymer. A tertiary amine was chemically attached to the polysulfone backbone polymer resulting in polymer-bound positive charge centers. Each polymer-bound positive charge center is counter balanced by a free moving counter anion. This anion is the hydroxide anion due to the critical role it plays in the zinc-air battery

chemistry. The end result is an ionomer that is charge neutral and capable of transporting hydroxide anions. Details regarding the synthesis, structure, and characterization of the ionomer are presented in the methodology section of this thesis.

The goal of this thesis is to advance human knowledge of ionomers for zinc-air battery cathodes. A detailed explanation of the synthesis of the ionomer is presented first followed by its characterization using NMR spectroscopy. Next, this thesis identifies several important material properties and discusses how to characterize these properties. Lastly, experimental results are presented and discussed and then concluded with recommendations for future research.

The key material properties that this document focuses on are the following: the ionic conductivity of the ionomer, the ion exchange capacity (IEC), the water retention capacity, the swelling ratio, the pore size and presence of pin holes in the ionomer membranes, the glass transition temperature, ionic conductivity improvement with salt doping, and the concentration and diffusivity of oxygen in the ionomer. All these properties yield important information regarding the performance of the ionomer being studied in this work. Additionally, the techniques described here can be applied to other ionomers for future research. A brief discussion of each property will be presented next; a more detailed discussion can be found in the theory and methodology section.

The ionic conductivity of the ionomer is perhaps one of the most important parameters that must be known for the development of a zinc-air battery. The ionic conductivity is a measure of the polymer's ability to conduct ions. Without proper ionic conduction, chemical reactions will occur very slowly or not at all. Therefore, the ionic conductivity of the ionomer must be great enough

so that the battery can perform at usable levels. If the ionomer fails to meet certain benchmarks, then it must be improved upon before the battery cell can be further developed. The ionic conductivity of the ionomer was measured using a four-point probe AC impedance technique. More specifically, potentiostatic electrochemical impedance spectroscopy was used. These measurements were performed on ionomer samples that were fully hydrated to find the maximum ionic conductivity possible.

Another important material property is the ion exchange capacity (IEC) of the ionomer. The IEC is a measure of the polymer-bound positive charge center density or ion exchange site density. In other words, it's the number of quaternary ammonium groups per gram of material. This property allows us to measure how functionalized the ionomer is and gives us a rough idea of the expected performance. Typically the higher the functionalization, the better the polymer will work as an electrolyte. The IEC is measured using an ion exchange bath and a pH probe.

The water retention capacity (WRC) is measure of the ionomers' ability to retain water at various relative humidity. As shown previously, water is an important species in the zinc-air battery chemistry and must be present in the ionomer. Thus it is important to know the water content of the ionomer at various relative humidity. The zinc-air battery has to be able to operate in various environments where the available air could be very dry or very humid. The water retention capacity was measured at various relative humidity including at its fully hydrated state. The measurements were made by following differences in mass gained/lost at different relative humidity.

The swelling ratio is an important parameter that measures the extent of swelling in the ionomer as it picks up or loses water from the atmosphere. Volume changes in the polymer due to water content will need to be known for the successful design off a zinc-air battery cell. In this work, the swelling ratio as a function of relative humidity was investigated and reported. More specifically, swelling in the diameter and thickness of round ionomer samples is shown. This information is closely related to the water retention capacity of the ionomer and will be useful in battery cell design. The swelling ratios were calculated from differences in measurements of the physical dimensions of several samples. Furthermore, these measurements were performed on samples that were equilibrated at various relative humidity.

The pore size and the presence of pin holes is a concern for the assessment of quality in the ionomer. The electrolyte needs to be able to prevent the diffusion of oxygen to the zinc anode. If oxygen reacts directly with metallic zinc to form zinc oxide, then it will defeat the purpose of an electrochemical cell. This would in essence be shorting out the battery chemically. Therefore, it is necessary to know the pore size and distribution within the ionomer. Additionally, polymer membranes must be checked to ensure they do not have any pinholes or macroscopic channels that would allow oxygen to reach the zinc anode directly. In this work, an optical microscope, scanning electron microscope (SEM), and a bubble point tester were used to characterize the pore size and presence of pin holes as best as possible.

The glass transition temperature is a temperature at which the polymer goes from a brittle-like state to a more rubbery state. This transition is not a phase transition however; it is merely a laboratory phenomenon. Nevertheless, it

is important to compare the operating temperature of the battery to the glass transition temperature. Polymers will have greater toughness when their internal temperature is higher than their glass transition temperature. This could be particularly advantageous for processing and manufacturing. If the internal or operating temperature of the ionomer is below the glass transition temperature, then plasticizers can be used to help lower the glass transition temperature and possibly provide better processability. Differential scanning calorimetry (DSC) was used to find the glass transition temperature of this ionomer.

One of the drawbacks to using an ionomer is that its ionic conductivity will be lower than what can be obtained using an aqueous or gel electrolyte. However, the ionic conductivity of the ionomer can be improved by doping it with a free salt mixture. More specifically, a hygroscopic free salt can be used to aid in water retention within the ionomer. The ionic conductivity as a function of free salt content was measured and reported in this work for a specific free salt mixture. The conductivity measurements were made using the same conductivity cell and technique that was previously mentioned. Improving the ionic conductivity of the ionomer will certainly be beneficial for battery cell design. Especially since a commercial zinc-air battery will need to operate a low relative humidity.

Lastly, this work investigated the concentration and diffusivity of oxygen in the ionomer. These measurements were performed for the same reason the pore size and distribution was investigated; to better understand if oxygen will be able to diffuse through the ionomer and react directly with the zinc anode. The measurements were made by using a combination of hydrodynamic voltammetry and chronocoulometry on a rotating disk electrode (RDE). The data gleamed

from these experiments were used to construct Koutecky-Levich and Anson plots. The y-axis intercept from the Koutecky-Levich plot and the slope from the Anson plot can then be used to calculate the concentration and diffusivity of oxygen in the ionomer. This technique serves to better understand the ionomer being studied but can also be used as a powerful tool for the characterization of future ionomers.

CHAPTER 2

LITERATURE REVIEW

Ionomers are receiving a great deal of attention these days in hopes of improving rechargeable battery and fuel cell technology. The ionomer that was studied in this work is responsible for transporting anions; specifically hydroxide anions. Polymers such as these are commonly known as alkaline anion exchange membranes (AAEM). These membranes are applicable to both batteries and fuel cells such as methanol fuels cells. AAEMs can be synthesized form many polymers, however the AAEM studied in this work is based off of a polysulfone backbone.

2.1 Literature Review of the Chloromethylation Reaction

A great deal of work has been dedicated to polysulfone based AAEMs due to its excellent chemical stability and mechanical strength [1, 2, 4, 6, 9, 10, 11, 13, 17, 21, 23-29, 33, 35-39, 62-66]. These ionomers are prepared by first chloromethylating the polysulfone and then quaternizing it. The chloromethylation reaction will chemically bond chloromethyl groups to the polysulfone back bone while the quaternization reaction will chemically bond tertiary amines to the chloromethyl groups. These reactions will be covered in detail in the theory and methodology section of this thesis. However, the reader should note that adding a tertiary amine to the chloromethyl group will cause the nitrogen atom in the substituent to carry a positive charge. It is this positive charge that allows the functionalized polymer to behave like an electrolyte. Furthermore, the positive charge will be counter balanced by an anion. This anion will be the chloride anion if the polymer has not yet been ion exchanged.

The chloromethylation reaction is typically done by one of two popular reaction schemes. The first reaction scheme, and perhaps the most effective, is done by using chloromethyl methyl ether as a chloromethylating agent and zinc chloride as catalyst [6, 9, 10, 11, 17, 21, 25, 27, 37]. These reagents have excellent conversion and product yield. The reaction time can vary from several hours to several days with an increase in product conversion as the reaction time is increased. They are usually performed in 5 weight percent solutions with 1,2-dichloroethane, chloroform, or 1,1,2,2-tetrachloroethane as solvents. However, it has been identified that chloromethyl methyl ether is a carcinogen and its use is highly discouraged [23].

The other reaction scheme for chloromethylation uses paraformaldehyde, chlorotrimethylsilane as the chloromethylating agent, and stannic chloride [Sn(IV)Cl] as the catalyst [1, 2, 4, 13, 23, 24, 26, 28, 29, 38]. This reaction is also carried out in 5 weight percent solutions and uses the same solvents as before. The downside to this reaction scheme is that longer times are required to achieve high conversion yields; typically 48 hours or more is used as the reaction time. However, these chemical reagents are considered far less hazardous to one's health. The ionomer studied in this work was synthesized using this safer reaction scheme.

A functionalized polysulfone AAEM can be created by starting with the base monomers that make up the polysulfone backbone [33, 35, 36, 39]. Polysulfone is polymerized from a condensation reaction using bis(4-chlorophenyl) sulfone and bisphenol A. The advantage of this method is that the individual monomers can be functionalized before they are polymerized and high degrees of functionalization can be achieved without the risk of crosslinking.

Crosslinking reactions occur when one polymer chain forms a chemical bond with another polymer chain making them permanently attached to each other. Crosslinking is typically undesirable because it makes the polymer insoluble. However there are a few instances when crosslinking is actually desirable [14, 33, 67]. Crosslinking will be explained more in detail in the theory and methodology section of this document. Lastly, starting from monomers makes it easier to create co-polymers with other polymers that can contribute desirable attributes, such as increased toughness, to the final product.

2.2 Literature Review of the Quaternization Reaction

The quaternization reaction is responsible for converting the chloromethyl group in to a methyl ammonium group [, 2, 4, 6, 9, 10, 11, 13, 17, 21, 23-29, 33, 35-39, 62-66]. This reaction is carried out in a high boiling point solvent such as N,N-Dimethylacetamide (DMAc), N,N-Dimethylformamide (DMF), 1-Methyl-2-pyrrolidone (NMP), and Dimethyl Sulfoxide (DMSO). Chloromethylated polysulfone is dissolved in one of these solvents and then a tertiary amine is added. Tertiary amines include trimethylamine, triethylamine, dimethylethylamine, dimethylisopropylamine, tetramethylethylenediamine, N,N,N',N'-tetramethylhexanediamine, and 1,1,2,3,3-pentamethylguanidine to name a few. The selection of the tertiary amine will have a direct effect on the chemical and physical properties of the ionomer. The reaction time will depend on the chemical reaction procedures but can be anywhere from a couple of hours to a couple of days. In addition to amine groups, phosphonium groups can be used instead to functionalize the chloromethylated polysulfone [13, 29]. These phosphonium groups, such as triphenylphosphonium and tris(2,4,6-

trimethoxyphenyl)phosphine, also have a positive charge which enables the transport of anions.

2.3 Polymer Membrane Casting Techniques

Once the polymer has been functionalized, it will need to be processed into a thin film or membrane. There are several ways of doing this [9, 21, 22, 23, 27, 28, 30, 31, 34, 35, 39, 68-72]. However, the most popular is to solution cast the material onto a flat surface. Typically a dilute solution, ca. 5 – 15 weight percent, of ionomer is prepared for casting. This solution is poured either into a pertri dish or drop-casted onto a glass, ceramic, or metal plate. The casting is allowed to dry for several hours and is sometimes heated in an oven for over a day to ensure that all of the solvent has been evaporated. For example, Abuin and coworkers would cast their ionomer onto a glass plate and allow it to dry in an oven at 70°C for 24 hours [9]. Yan and coworkers also cast their polymer onto a glass plate but allowed their membranes to dry at 40°C for 72 hours [30]. Once these AAEMs are completely dry, they are peeled off from their substrate; sometimes with the assistance of deionized water.

2.4 Ion Exchanging

The counter anion for most, if not all, of the polymer castings will be the chloride anion since the chloromethyl group was used to functionalize the polymer. The chlorine atom in the chloromethyl group gets detached by the attacking tertiary amine and becomes an anion that counter balances the newly formed positive charge on the amine group. Because of this chloride anion, the ionomer or AAEM is said to be in the chloride form. Alkaline metal-air batteries and fuel cells will require the ionomer to be in the hydroxide form meaning that the counter anion needs to be a hydroxide anion. In order to exchange the

chloride anion for the hydroxide anion, the ionomer will need to be soaked in an exchange bath [5, 9-12, 14, 17, 21, 22-23, 27, 30, 31, 39]. The exchange baths are typically sodium hydroxide or potassium hydroxide aqueous solutions. Their concentration varies from group to group but typical concentrations are 1 to 8 molar. The time that the membranes are allowed to soak in the exchange baths also varies from group to group but the average time is 24 hours. After the exchange process is complete, the membranes are thoroughly washed with deionized water to thoroughly remove excess alkaline salts. The polymer membranes are ready for testing and characterization once they have been exchanged into the appropriate anion.

2.5 Ionic Conductivity

One of the most important properties of the AAEMs is its ionic conductivity. The ionic conductivity is a measure of the membrane's ability to transport ions. The method of measuring the ionic conductivity is highly studied and applicable to many materials [1, 2, 5, 7-12, 16, 17-23, 25, 27, 30-33, 35, 39, 43-50, 73-80]. Measuring the ionic conductivity of an ionomer involves using an ac-current impedance spectroscopy technique with special equipment such as a conductivity cell and frequency response analyzer. The conductivity cell can have either two probes [8, 9, 18, 19, 20, 22, 31, 32, 39] or four probes [1, 2, 5, 10, 11, 12, 17, 21, 23, 25, 27, 30, 35, 45]. The work presented in this thesis used a conductivity cell with four probes and more specific information regarding this measurement is provided in the theory and methodology section of this thesis. Detailed information provided by BekkTech was very helpful in conducting the experiments [44, 46, 47, 48]. The cells can be tested in various environments with differing temperature and relative humidity. However, testing is generally

done under deionized water and at room temperature. Testing at higher temperatures generally reveals that the ionic conductivity of polysulfone based AAEMs increases with increasing internal temperature. The same can be said about the water content within the AAEM. Yan and coworkers show that room temperature ionic conductivities in deionized water for various ionomers vary from 1.6 to 53 mS/cm [17]. In their work, the highest ionic conductivity (53 mS/cm) was achieved by an imidazolium functionalized polysulfone membrane while the lowest ionic conductivity was achieved by a quaternary ammonium functionalized polysulfone membrane. Indeed, most AAEMs presented in this literature review fall within this range when measured at room temperature and deionized water.

2.6 Ion Exchange Capacity

The ion exchange capacity (IEC) is another important property studied in this work. This property is a measure of the polymer-bound positive charge center density in the AAEMs. In other words, this property tells us how many functionalized molecules there are per unit mass of material. This property can be found using the back titration method [5, 8, 14, 17, 18, 21, 23, 30, 32, 33, 35, 36, 37, 39, 81]. The back titration method involves using a hydroxide form ionomer and ion exchanging it back into the chloride form in a sodium chloride bath of known volume. The released hydroxide anions are then titrated with a dilute acid such as 0.1M hydrochloric acid. The number of hydroxide ions released from the polymer sample can then be calculated using the titration data. Finally, the polymer sample is dried out completely and its mass is recorded. The IEC is calculated by dividing the moles of released hydroxide anions by the dry mass of the polymer sample. Additionally, the IEC can be found by ion

exchanging to the chloride form using 0.1M HCl and titrating the exchange bath with 0.1M NaOH or KOH. However, this procedure will require the titration of a standard 0.1M HCl solution so that the difference in volumes required for titration can be used in calculations. The unit of IEC is typically mmol/g. The IEC will depend on the conversion yield of both the chloromethylation reaction and the quaternization reaction. Therefore, the IEC is a useful parameter in determining the effectiveness of operating conditions in both chemical reactions. Because the IEC is highly dependent upon the conversion yields of both reactions, a wide spread in values can be seen in literature data for various ionomers. For example, Yan and coworkers found that their ionomer had an IEC of 2.19 mmol/g while the theoretical value for their polymer was 2.24 mmol.g [17]. Their results showed that the experimentally measured value was very close to the theoretical maximum for their polymer. This is an indication that they have adequately optimized their reaction conditions. In contrast, Hibbs *et al* reported the IEC of their ionomer to be 1.89 mmol/g while the theoretical maximum is 2.50 mmol/g [39]. Their results indicate that their reaction conditions can be further optimized to improve the IEC of their ionomer.

2.7 Water Retention Capacity

The water retention capacity (WRC) is an important material property that is relatively easy to measure. The WRC is a measure of the polymer's ability to absorb water. This property is frequently reported along with other common AAEM properties in the literature [2, 5, 8, 9, 11, 14, 17, 18, 19, 21, 23, 25, 30, 32, 33, 35, 36, 37, 39, 81]. The WRC is found by measuring the mass of a fully hydrated sample and the mass of a fully dehydrated sample. The two masses are subtracted from each other to find the water content of the sample. The water

content is then divided by the mass of the dry sample and multiplied by 100%. The exact procedure for drying and humidifying a polymer sample varies in the literature. However, samples are commonly allowed to soak in deionized water for a day or more. Drying is usually done in a vacuum oven and a predetermined temperature; however other methods are used as well. For example, Wang *et al.* dry their membranes in a nitrogen filled container at 55°C for 1 hour [2]. Zeng and coworkers will dry their membranes in a vacuum oven set to 60°C until a constant dry weight is achieved [8]. Lastly, Park *et al.* dry their membranes in a vacuum oven set to 110°C until constant weight is achieved [11]. The amount of water that a membrane can absorb is largely dependent upon the choice of polymer-bound functional group and the counter anion. Therefore, WRC values will vary from material to material even if the polymer backbone is the same. For example, Wang and coworkers report that the pristine version of their ionomer has a WRC of 81% ±4% [2]. Yan *et al.* report a range of WRC from 11% to 161% for the various ionomers they tested [17]. Lastly, Park and coworkers observed a WRC range of 5% to 25% for their ionomer [11]. These are examples of variance in WRC values reported in the literature. All three groups were working with polysulfone based ionomers.

2.8 Swelling Ratios

A property that is very closely related to the WRC of an ionomer is the swelling ratio. The swelling ratio is a measure of the expansion or contraction that an AAEM can undergo when it picks up or loses water. As explained previously in the introduction, this is an important polymer property that needs to be considered in both battery and fuel cell design. This value is also commonly studied in the literature [2, 5, 7, 17, 18, 20, 21, 33, 35, 82]. Typically, a physical

dimension of the polymer sample, such as the thickness or diameter, is measured when the sample is fully hydrated and fully dehydrated. The difference between the hydrated and dehydrated measurement is divided by the dehydrated dimension measurement and multiplied by 100%. The swelling ratio, similarly to the WRC, will depend on the specific material being studied. Using different counter anions or functional groups will have drastic effects on the swelling ratios. For example, Yan and coworkers reported swelling ratios that varied from 5% to 40% along the length of various samples [17]. Wang *et al.* saw a thickness swelling ratio of 61% ±3% in the pristine version of their ionomer [2]. Lastly, Zhao and coworkers reported area swelling ratios in the range of 0.30% to 0.80% for various polymer samples [33]. These examples are all based on a polysulfone backbone and emphasize that the swelling ratio can be reported for various dimensions.

2.9 Porosity

As explained in the introduction, the porosity of the ionomer is an important parameter to know. Having large pore structures in the AAEMs is undesirable in both metal-air batteries and fuel cells since oxygen diffusion and methanol fuel crossover will significantly reduce the performance of the device [15, 19, 32]. Porosity and pore structure were studied in the following works and their methods are applicable to the polymer studied in this thesis [7, 14, 15, 19, 20, 28, 32, 37, 59, 60, 61]. Perhaps the most popular way of characterizing the pore structure of an AAEM is to use scanning electron microscopy (SEM) to take high resolution photographs of the pores present in the membranes. SEM images can show physical details with resolution in the nanometer range. For

example, figure 2 is a high resolution SEM photograph of a polysulfone based polymer membrane showing details in its pore structure [59].

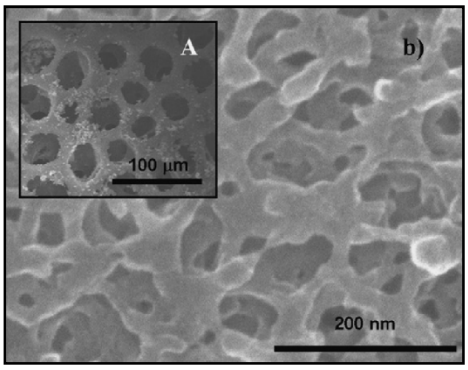

Figure 2. SEM image of a polysulfone-based membrane showing its pore structure. The inset shows larger pores that were present in the same sample.

Taurozzi *et al.* explain that the pores shown in figure 2 range from 30-100nm in size and have irregular shapes [59]. However, larger pores were found on the opposite side of the membrane and have a more regular shape. These pores, shown in the inset of figure 2, have diameters in the range of 20-50μm. The work of Taurozzi *et al.* is one typical example of how SEM images can be used to measure the size and distribution of pores in an ionomer membrane. However, more advanced techniques such capillary flow porometry can also be used to determine pore size [61].

2.10 Glass Transition Temperature

The glass transition temperature is another important property that is frequently investigated in AAEMs [22, 24, 40, 41, 43, 49]. The glass transition temperature of a polymer can change when different functional groups are attached. Even the counter anion in an AAEM can have an effect on the glass transition temperature. Differential scanning calorimetry (DSC) is typically used to measure the glass transition temperature of a polymer sample because these measurements are easy to perform, are relatively fast, and very repeatable.

Modern day software makes data processing and the assignment of glass transition values as very simple task. However, one important note should be taken; the glass transition temperature occurs over a range of temperatures and there are multiple methods of defining it. The American Society for Testing and Materials (ASTM) offers testing standards that guide researchers through experimental procedures and the assignment of glass transition temperatures. Indeed, ASTM standard E1356-08 was used as an aid in the investigation presented in this thesis [83]. Cozan and coworkers used DSC to investigate the glass transition temperature of their modified chloromethylated polysulfone polymer [24]. They heated their sample in a Mettler TA Instrument DSC 12E from 20°C to 250°C at a heating rate of 20°C/min. They cycled through the heating range once before determining the glass transition temperature on the second cycle. Cozan and coworkers investigated various polymer samples with differing degrees of chloromethylation. Their DSC work reports that the glass transition temperature varies from 158°C to 183°C and their data suggests that the glass transition temperature of their polymer samples is inversely proportional to the degree of chloromethylation. In other words, we can expect to see a decrease in glass transition temperature with increasing degree of chloromethylation.

2.11 Free Salt Addition to Ionomers

As stated previously, ionomers and AAEMs tend to suffer from low ionic conductivities when they are not fully hydrated. However, one work around to this problem is to dope the polymer with free salts that aid in boosting room temperature ionic conductivity. This type of work is being studied by several research groups [7, 20, 34, 49]. For example, Qiao and coworkers were able to achieve a maximum ionic conductivity of 530 mS/cm by doping their polymer

electrolyte in 8M aqueous KOH solution [7]. They reported that their polymer electrolyte retained its mechanical integrity and ionic conductivity for greater than one month. Doping ionomers is also commonly done in lithium polymer batteries [34]. These batteries utilize a polymer membrane matrix that has been soaked in a lithium salt solution. A very wide electropositive window can be achieved when lithium metal is coupled to such an ionomer. The end result is that high energy and power densities can be achieved [34].

2.12 Concentration and Diffusivity of Oxygen in Ionomers

The concentration and diffusivity of oxygen in an ionomer are key properties that must be known for the successful design of a metal-air battery cell. As such, it was surprising to see that no published literature data regarding oxygen concentration and diffusivity in quaternized polysulfone membranes could be found at the time of writing this document. However, these measurements have been performed for other polymers, mainly Nafion [52, 54, 55, 56, 57]. Rotating disk electrodes (RDE) and rotating ring disk electrodes (RRDE) were used in these works to study the oxygen reduction reaction. The electrolytes were mainly oxygen saturated dilute acids such as H_3PO_4, H_2SO_4, and $HClO_4$. Thin films were applied to platinum disk electrodes so that oxygen transport kinetics could be studied. Even though the polymers and electrolytes used in these works are completely different from the system studied in this thesis, their experimental procedures are still applicable. The work performed by Lawson *et al.* was instrumental in finding the oxygen concentration and diffusivity in the ionomer studied in this thesis [54]. Lawson *et al.* used an RDE to investigate the concentration and diffusivity of oxygen in Nafion. Their work discussed experimental procedures including thin film casting onto a platinum disk. Their

working electrolyte was oxygen saturated 0.7M H_3PO_4. Lawson *et al.* used a combination of chronocoulometry and hydrodynamic voltammetry to generate Anson and Koutecky-Levich plots from the raw data. These plots were then used to calculate the concentration and diffusivity of oxygen in the 0.7M H_3PO_4 and Nafion films. Their technique was used in this work to find the same values. As such, a detailed theory is provided in the theory and methodology section of this thesis. Lawson *et al*. report that the concentration and diffusivity of oxygen in oxygen saturated 0.7M H_3PO_4 is 1.3 ±0.1 mM and (1.5 ±0.1)x10^{-5} cm^2/s respectively. Furthermore, they report these values to be 3.8 ±0.1 mM and (0.2 ±0.1)x10^{-5} cm^2/s in their Nafion film. They concluded that the concentration of oxygen was greater in the Nafion film than in solution; although, oxygen had a smaller coefficient of diffusion in the film than it did in the solution. In addition to the work done by Lawson *et al.* the following references were also helpful in conducting the experiments presented in this thesis: references 51, 52, 53, 55, 56, 57, and 58.

CHAPTER 3

THEORY AND METHODOLOGY

3.1 Synthesis of Chloromethylated Polysulfone

The ionomer is synthesized from a basic polysulfone polymer through the use of two specific chemical reactions. The first chemical reaction is known as the chloromethylation reaction and serves as a preparation for the second chemical reaction. The chloromethylation reaction will chemically bond chloromethyl pendant groups to the polysulfone backbone; hence it's given name. These chloromethyl groups are then modified in the second chemical reaction known as the quaternization reaction. This reaction is responsible for turning the polymer into a functional electrolyte by chemically attaching positive charge centers. Each positive charge center is counter-balanced by a free anion to maintain electro-neutrality. The end result is a material that contains polymer bound positive charge centers that are able to transport free anions across its chains.

The author of this work closely followed the procedure outlined by Avram *et al.* [62]. The chloromethylation reaction is started by dissolving 30 grams of polysulfone (67.79mMol) in 1 liter of chloroform at room temperature. 10 molar equivalents of paraformaldehyde (677.9mMol, 20.36g) are added to the reaction vessel. The contents will turn cloudy white and the paraformaldehyde will not fully dissolve. Next, 10 molar equivalents of chlorotrimethylsilane (677.9mMol, 73.65g, 86.04mL) are slowly poured into the reaction. Lastly, 0.088 molar equivalents of tin tetrachloride catalyst (5.982mMol, 1.56g, 0.70 mL) are carefully added drop wise into the reaction mixture. The reader should note that Avram *et al.* used 0.1 molar equivalents of tin tetrachloride catalyst. However, it was found that 0.1

molar equivalents are very prone to cause crosslinking during the reaction; crosslinking will be explained in the paragraphs that follow. Using 0.088 molar equivalents is recommended as this minimized crosslinking in the chloromethylation reactions. The addition of the catalyst will begin the chemical reaction and the contents will fully dissolve as they are heated and stirred. This reaction was heated to 52°C for a total of 48 hours with continuous stirring. The reaction mixture should be transparent by the time its internal temperature reaches 52°C. In other words, all chemical reagents should be fully dissolved. Over the course of 48 hours, the color of the reaction will change to a light brown or tan color.

It should be noted that increasing the reaction temperature above 52°C will promote crosslinking of the polymer chains. Crosslinking occurs when chemical bonds are formed between adjacent polysulfone chains. Generally, the degree of crosslinking will increase as the reaction temperature is increased. Additionally, overloading the reaction with catalyst will also promote a higher degree of crosslinking. It is therefore recommended that no more than 0.1 molar equivalents of tin tetrachloride catalyst be added. It is better to be just shy of 0.1 molar equivalents than to go over. In general, crosslinking is an undesirable result since the material cannot be functionalized in the second chemical reaction and cannot be reversed. Any crosslinked material will have to be removed in the steps that follow. An example of crosslinking during chloromethylation and quaternization is shown in figure 3 [10].

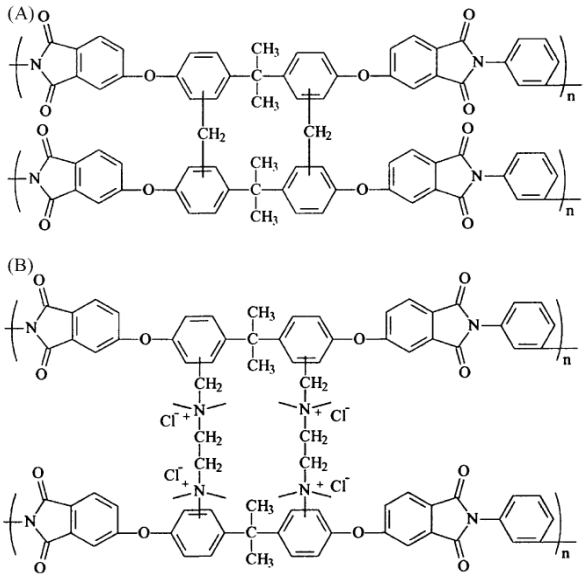

Figure 3. An example of crosslinking in (A) the chloromethylation reaction and (B) the quaternization reaction.

The chemical reaction is terminated by quenching the reaction contents in an anti-solvent system. For this reaction that anti-solvent system is 1 liter of 70% reagent grade ethanol, 30% deionized water. The purpose of the anti-solvent is to force the chloromethylated polysulfone (CMPSU) out of solution. Additionally, the anti-solvent will remove excess chemical reagents dissolved in the reaction mixture. The new mixture will form a very cloudy solution with white color. The mixture should now be allowed to sit at room temperature without agitation for a full 24 hours. The polymer will collect into a solid gel-like substance at the bottom of the anti-solvent container. This substance will have a light-tan color. The liquid, which will be mostly chloroform, ethanol, and water should be decanted completely from the container and discarded. The polymer should be immediately purified again by dissolving the solid mass in 1 liter of fresh chloroform. The chloroform should be boiled for 30 minutes. Any solids that remain after boiling in chloroform for 30 minutes will most likely be crosslinked

material. This substance can be removed by allowing the chloroform to cool to room temperature and then pouring over filter paper. Once the crosslinked material has been removed, the chloroform can then be mixed with 1 liter of fresh anti-solvent solution to force out the chloromethylated polysulfone again. The newly purified polymer will also have a tan color, albeit much lighter than the first. The primary purpose of the second purification step is to remove any crosslinked material. However, this step also serves the purpose of removing excess chemical reagents from the chloromethylation reaction that were not removed during the first anti-solving step. After anti-solving for the second time, the chloromethylated polysulfone should be allowed to collect for another 24 hours. Once again, the polymer will form a gel-like substance with light tan color at the bottom of its container.

The next step in the process is to decant and discard the anti-solving solution and collect the polymer. At this point, the material will be saturated with chloroform, ethanol, and water. These liquids need to be removed with a vacuum oven. The polymer should sit in the vacuum oven set to 50°C and maximum vacuum until all liquids have been expelled. The mass of the polymer should be checked periodically until constant weight is achieved. A 30 gram batch of chloromethylated polysulfone will typically achieve constant weight, and thus indicating complete dryness, within 24 hours. Once dry, the polymer can be stored in any container and is ready for use in the second chemical reaction. However, before any material is used, it is important to characterize the extent of chloromethylation of the polysulfone polymer chains.

The extent of chloromethylation, or better known as the degree of chloromethylation, is characterized by nuclear magnetic resonance (NMR)

spectroscopy. The degree of chloromethylation can be calculated directly from NMR spectra. A higher degree of chloromethylation is more desirable than a lower one since the chloromethyl groups will be changed into polymer-bound positive charge centers in the quaternization reaction. The more polymer-bound positive charge centers the material has, i.e. greater charge density, the better its ionic properties could be. In other words, the ionomer might have a greater ionic conductivity if the degree of chloromethylation is maximized. For a metal-air battery, having maximum ionic conductivity is definitely desirable.

The maximum theoretical degree of chloromethylation that can be achieved on polysulfone is 200% [10]. 200% chloromethylation corresponds to having 2 chloromethyl groups on each polysulfone monomer as shown below in figure 4 [1].

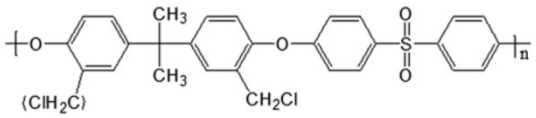

Figure 4. 200% chloromethylated polysulfone.

The degree of chloromethylation was found to have a direct relationship with the reaction time and catalyst loading. For example, using a catalyst loading greater than what was previously recommended had the direct effect of yielding batches of polymer with greater degree of chloromethylation. In addition, increasing the reaction time beyond 48 hours will also have the direct effect of increasing the degree of chloromethylation in the polymer. However, attempting to increase the degree of chloromethylation of the polymer by increasing either the reaction time or catalyst loading will run the risk of increasing the amount of crosslinking. As was stated before, crosslinked material is useless for this application since it

cannot be quaternized. Interestingly enough, it was found that increasing the reaction temperature above 52°C while holding everything else constant did not improve the degree of chloromethylation. On the contrary, it was found that operating above 52°C would make it difficult to predict the outcome of the reaction. Drastically different degrees of chloromethylation resulted from reactions that were ran in parallel with exactly the same reagent quantities. It should be noted that the purpose of this work was not to optimize the chloromethylation reaction but to characterize the ionomer. Further research will be required for investigating optimal operating conditions and their effects on the performance of the ionomer.

Once a batch of chloromethylated polysulfone has been fully processed, an NMR spectra of the material should be obtained. Preparation of NMR samples is very straight forward. One should cut a sample of ca. 30 milligrams from the batch of chloromethylated polysulfone and dissolve it in 1-1.2 milliliters of deuterated chloroform. Agitation and heat will help the material dissolve faster in the deuterated chloroform. However, it was found that leaving the material to soak in the solvent overnight would work equally as well. It is critical that no solid particles remain once the sample is ready to be injected into an NMR tube for testing. Filter the solution over glass wool if necessary. Once the NMR sample has been prepared and stored in an NMR tube, an NMR test should be conducted as soon as possible in order to minimize solvent loses due to evaporation. Figure 5 below is the NMR spectra of the chloromethylated polysulfone used in this research work.

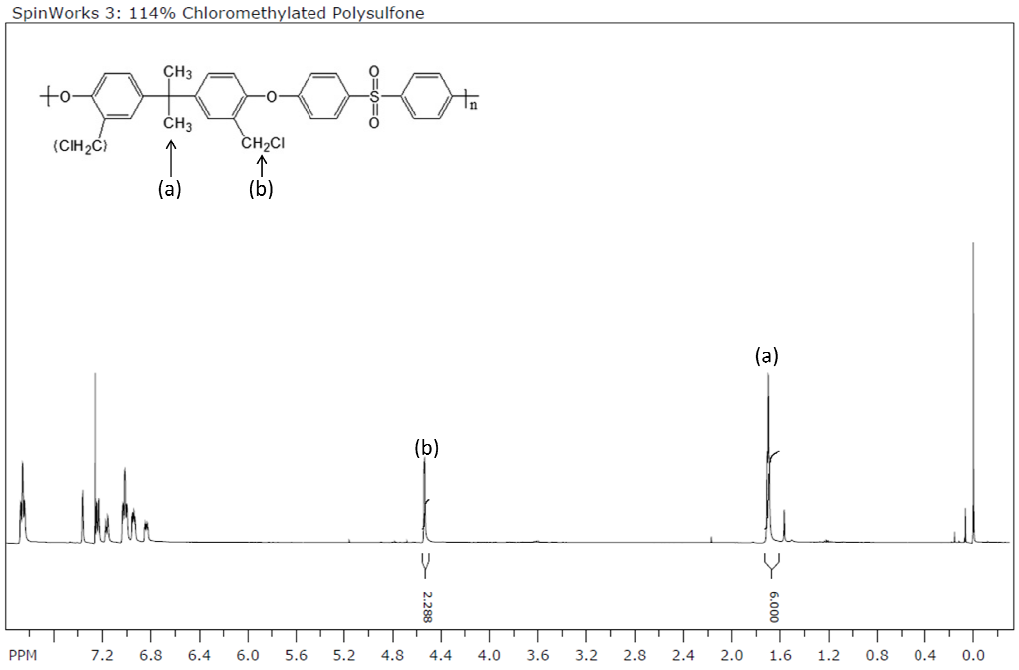

Figure 5. NMR spectra of 114% CMPSU. Peak (a) corresponds to the isopropylidene group. Peak (b) corresponds to the chloromethyl group.

The degree of chloromethylation can be calculated directly from the NMR spectra. Firstly, all signals need to be normalized to a reference value. The author of this work chose to set the area integral of the isopropylidene group of polysulfone to 6. This is signal (a) in Figure 5. Next, the area integral of the chloromethyl peak is used to calculate the degree of chloromethylation. Peak (b) in Figure 5 corresponds to the chloromethyl groups on the polysulfone backbone. The degree of chloromethylation is calculated from the following equation:

$$DOC = \frac{Chloromethyl\ Peak}{2} * 100\%$$

The degree of chloromethylation can be thought of as the number of chloromethyl groups per 100 polysulfone monomers in a polymer chain. Additionally, it is assumed that all polysulfone monomers will have at least one chloromethyl group before any receive a second. For example, a polymer that has a degree of chloromethylation of 50% indicates that out of 100 polysulfone

monomers, only 50 of them have one chloromethyl group. A degree of chloromethylation of 100% indicates that out of 100 monomers, all 100 will have one chloromethyl group. A polymer with a degree of chloromethylation of 150% indicates that out of 100 polysulfone monomers, 50 will have 1 chloromethyl group and the other 50 will have 2 chloromethyl groups. Finally, a polymer that has a degree of chloromethylation of 200% will have two chloromethyl groups on all 100 polysulfone monomers. Using the above equation, we can see that the material used in this work has a degree of chloromethylation of 114%. This means that out of 100 polysulfone monomers in a polymer chain, 86 monomers will have 1 chloromethyl group and 14 monomers will have 2. This logic can also be applied in terms of percentages. For example, in 114% chloromethylated polysulfone, 86% of all monomers in a batch will have 1 chloromethyl group and 14% of all monomers will have 2 chloromethyl groups.

The molecular weight of any chloromethylated polymer can be calculated by averaging the molecular weights of polysulfone (442.53 g/mol), 100% chloromethylated polysulfone (490.00 g/mol), and 200% chloromethylated polysulfone (539.47 g/mol). For example, the molecular weight of the 114% chloromethylated polysulfone used in this work is calculated as follows:

$$114\%\ CMPSU = (0.14) * \left(539.47 \frac{g}{mol}\right) + (0.86) * \left(490.00 \frac{g}{mol}\right) = 497.78 \frac{g}{mol}$$

Therefore, the molecular weight of the chloromethylated polymer used in this work is 497.79 g/mol. This procedure can be used to calculate the molecular weight of any chloromethylated polysulfone polymer up to 200% degree of chloromethylation, the theoretical limit.

3.2 Synthesis of Quaternized Polysulfone

The characterization of the chloromethylated polysulfone is concluded once the degree of chloromethylation is calculated. The polymer can now be used in the quaternization reaction. The goal of the quaternization reaction is to chemically bond a positive charge center to the polysulfone backbone. The positive charge center is formed when a tertiary amine replaces the chloride atom in a chloromethyl group. Tertiary amines are functional groups composed of a nitrogen atom with a lone pair of electrons and three organic substituents. The nitrogen atom becomes positively charged when its lone pair of electrons makes a chemical bond with the methyl group and replaces the chloride ion. Once this reaction occurs, the polymer becomes a functional electrolyte.

The reaction is started by assembling a reaction vessel and pouring in 1 liter of N,N-Dimethylformamide (DMF). 10 grams of chloromethylated polysulfone is then introduced into the reaction vessel. More or less material can be used as long as the volume of DMF is adjusted such that the weight percent of the chloromethylated polysulfone in solution is ca. 1 weight percent. Next the tertiary amine is introduced into the reaction vessel. The moles of tertiary amine added should double the total moles of chloromethyl groups present as determined by the degree of chloromethylation. In this work, 2.2x moles of tertiary amine were used for quaternization. The tertiary amine used in this work cannot be stated since it is currently a trade secret material of Fluidic Energy, Inc. However, this tertiary amine was chosen for its excellent stability in alkaline media. After the addition of the tertiary amine into the reaction vessel, the DMF solvent is then sparged with argon gas for 1 hour by bubbling directly into the liquid. The purpose of argon sparging is to remove any dissolved gases such as oxygen.

Sparging with argon is maintained throughout the reaction. After sparging for at least 1 hour, heat is applied to the reaction so that the DMF solvent is brought to a boil (ca. 152-154°C). The reaction is maintained at a boiling temperature for a full 24 hours. Once 24 hours have passed, the reaction is terminated by allowing it cool to room temperature. At this point, argon sparging can be discontinued. A synthesis schematic for both the chloromethylation and quaternization reaction are shown in a figure 6 [10]. Additionally, figure 6 also shows the alkalization of the ionomer that is accomplished with an anion exchange bath.

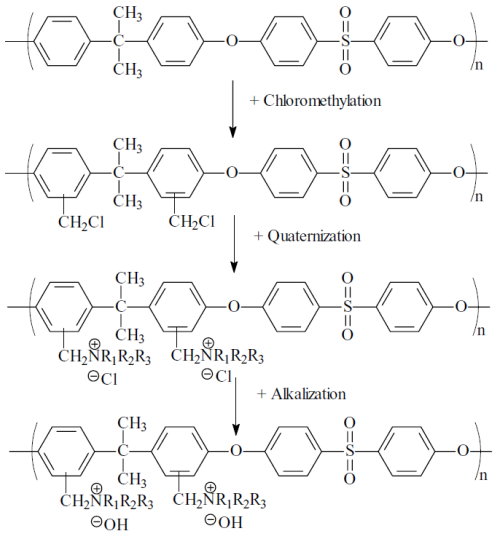

Figure 6. Chemical reaction scheme for the chloromethylation and quaternization of polysulfone. The alkalization of quaternized polysulfone is also shown.

Similarly to the chloromethylation reaction, crosslinking can also occur during the quaternization reaction. This crosslinked material must also be removed since it is not ionically conductive. The removal process is straight forward and less tedious than the process for removing crosslinked material from the chloromethylation reaction. Firstly, the quaternized polymer solution needs to be concentrated from 1 weight percent to 15 weight percent. This can be accomplished quickly by using a vacuum oven that accelerates the evaporation

of DMF. However, the author of this work typically prefers to evaporate the solvent completely by pouring the solution into Petri dishes and letting them sit overnight on a hot plate set to 50°C. The advantage of this process is that dried polymer solid can be stored more easily than a liquid solution. Additionally, the researcher can choose how much material to use for purification. If working from dry solid polymer material, then all that is needed to be done is re-dissolve the polymer in fresh DMF and concentrate to 15 weight percent.

The next step is to centrifuge the 15 weight percent solution. Centrifugation will bring crosslinked material, which is insoluble in DMF, to the bottom of the container. The crosslinked material will clump into one large mass. The author of this work found that spinning the sample at 6000 revolutions per minute for 10 minutes will produce more than adequate results. After centrifugation, a glass pipette, or similar instrument, can be used to suck the clean liquid material from the top and transfer it to a storage container. The researcher can also choose to decant the clean polymer solution and leave the crosslinked material behind in the centrifuge container. However, this is not recommended because if the liquid solution is too viscous, then pouring the solution may be time consuming, especially if the centrifuge container volume is very large in comparison to the volume of the clean polymer solution. On the other hand, if the solution is not viscous enough, then some crosslinked material may flow with the clean solution. There may be other separation techniques as well; however, the author of this work found that using a glass pipette is fast, simple, and efficient. Once a clean polymer solution is obtained it can then be cast into membranes or stored for future use. Casting techniques will be discussed in the next section.

3.3 Casting Ionomer Membranes

There are several methods of casting ionomer membranes as discussed in the literature review; however, the author prefers to prepare free standing membranes by using a drop-casting technique. A drop cast membrane is prepared by dropping a polymer solution from 1-2 inches above a flat surface such as a glass, ceramic, or metal plate. The author found that optically-flat quartz glass plates make the best membranes. Additionally, regular glass plates also work well but make the removal of free standing membranes more difficult. The solution should be cast onto the glass plates drop wise with a glass pipette making sure to spread the material evenly and cover the desired surface area. The researcher should ensure that the glass plates are perfectly leveled before drop casting to prevent thickness differentials throughout the membrane. The thickness of the membranes can be controlled by altering the weight percent of the polymer solution. If a thin membrane is required, then a dilute solution should be used. If a thicker membrane is needed, then a more concentrated solution should be used. The author found that a 15 weight percent solution will make membranes with a thickness in the range of ca. 150 – 200 micrometers.

Once the membrane has been cast out, it should be left to dry in air at room temperature. Complete evaporation of the DMF solvent typically requires a full 24 hours in ambient conditions (27°C, 20% relative humidity). Heat should not be applied to the membranes for accelerating the evaporation of the solvent since it could cause defects in the final product. Heated membranes tend to have a greater amount of trapped air bubbles and wrinkles on the surface. After a full 24 hours of drying, the membranes can be removed from the glass plates by immersion in water. Immersion for 1 hour in a clean water bath should suffice for

the removal process. The membranes will soak in some water and cause minor delamination due to the expansion of the material. Additionally, the water acts similarly to a plasticizer and will increase the toughness of the polymer membranes. This is beneficial since these polymer membranes can be very brittle when dry and will easily crack if the removal process is too forceful. In the case of the quartz glass plates, all that is needed to be done is to lift an edge up from the surface of the glass using a razor blade and gently peel off the remainder of the polymer membrane. If regular glass plates are used, then the razor blade may be needed to remove the membrane entirely off of the surface of the glass. Once membranes are removed from the glass plates, they can be stored under water to keep them ductile.

3.4 Measurement of the Ionic Conductivity

The ionic conductivity of the ionomer was measured using a four-point probe conductivity cell coupled with potentiostatic electrochemical impedance spectroscopy (PEIS). The cell was connected to a Garmy Instruments Reference 3000 potentiostat and AC impedance measurements were carried out at frequencies between 0.1Hz to 300kHz. Samples of ionomer are punched out from drop cast membranes using a punching tool. Each punch will produce 4 identical samples from a single casting and each sample will measure 30mm x 5mm. The conductivity cell is made of up of two Teflon squares with channels cut into them so that the polymer sample can equilibrate with a controlled environment. A picture of the conductivity cell is shown below in figure 7.

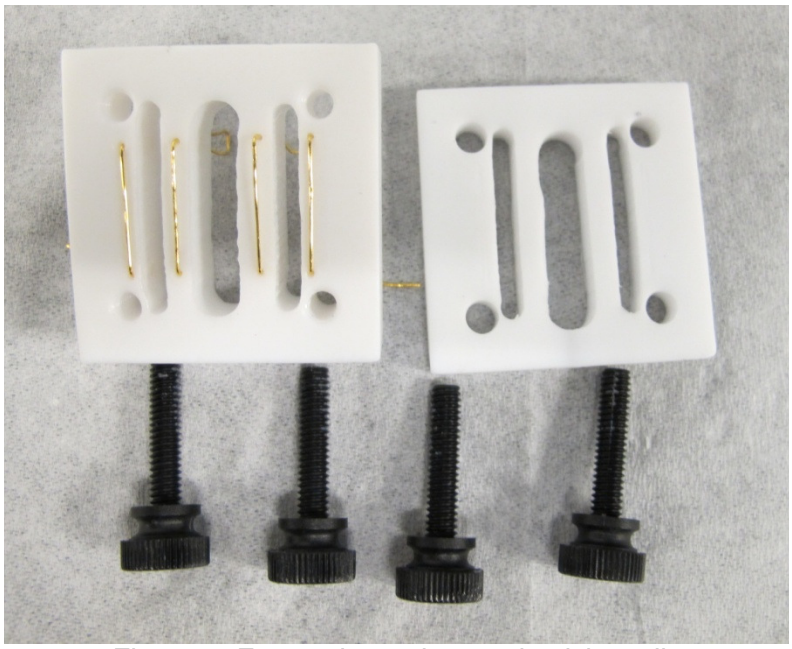

Figure 7. Four-point probe conductivity cell.

Four gold wires were used as electrodes and have been threaded through small holes that were cut into the Teflon. These gold wires serve as the four points of contact in conductivity testing. The polymer samples are laid horizontally on the four gold wires and are held tightly against them by clamping the second half of the conductivity cell with thumb screws. The outer two gold wires will apply an electrical current while the inner two gold wires will measure the voltage potential between them. PEIS data is plotted in the form of a Nyquist plot and used to find the resistance of the ionomer. The resistance is given by the right side semi-circle intersection with the horizontal axis. The ionic conductivity of the ionomer can then be calculated using the measured resistance and the dimensions of the polymer sample. The following formula is used for calculating the ionic conductivity:

$$\sigma = \frac{l}{R * w * t}$$

In the above equation, σ is the ionic conductivity and its units are Siemens per centimeter (S/cm). The variable l is the length of the membrane in between the two voltage sensing electrodes and is measured in centimeters. The variable R is the resistance of the membrane as found from the PEIS experiments and has units of ohms (Ω). Lastly, the variables w and t are the width and thickness of the membrane samples respectively and have units of centimeters**.** Testing is performed in a humidity chamber where the temperature and relative humidity can be held at a constant value. Additionally, testing can be done in ultrapure Millipore water in order to find the maximum ionic conductivity of the polymer samples. According to EMD Millipore, the water processed by the Milli-Q Advantage A10 water purification system has a resistivity of 18.2 MΩ*cm at 25°C. In this work, the ionic conductivity of the ionomer was found under fully hydrated conditions in order to find the maximum. This was performed for the chloride and hydroxide form of the polymer. The Nyquist plots are difficult to interpret at any relative humidity that is below fully hydrated conditions and will thus yield unreliable conductivity measurements. However, an additional experiment was preformed where free salt was added to the ionomer in order to boost its ionic conductivity and measurements were successfully taken at 50% relative humidity.

3.5 Measurement of the Ion Exchange Capacity

The ion exchange capacity (IEC) is the number of polymer bound positive charge centers per gram of material. It has units of millimole per gram (mmol/g). This measurement gives insight into the functionality of the ionomer and provides for an easy way of estimating the degree of quaternization, i.e. the extent to which chloromethyl groups were converted into quaternary ammonium cations. If

100% conversion is achieved in the quaternization reaction, then the measured IEC should be equal to the theoretical IEC as this would imply that all of the chloromethyl groups were converted. The theoretical IEC can be calculated using the degree of chloromethylation. If anything less than 100% conversion is achieved, then the measured IEC will be less than the theoretical IEC. Thus a basic estimation of conversion can be obtained by taking the ratio of the measured IEC to the theoretical IEC.

The process is started by first ion exchanging a polymer sample from the chloride form to the hydroxide form. In this work, polymer samples were immersed in a 2M KOH bath for 48 hours at room temperature. Next the polymer samples are immersed in a large ultrapure Millipore water bath for 24 hours. The purpose of this step is to remove any excess KOH from the polymer samples as much as possible. Lastly, the polymer samples are each immersed in their own 3M KCl bath of known volume for 48 hours to exchange the polymer back into the chloride form. It is very important that the volume of the 3M KCl bath is precisely known for calculating the ion exchange capacity. The author used 220mL of 3M KCl solution for polymer samples whose dry mass is in the range of 0.5 – 1g.

At the end of 48 hours in the 3M KCl bath, a pH probe is used to measure the pH of the solution directly; the polymer sample should not be removed from the solution during measurement. The only source of hydroxide anions will be from the polymer sample. The total number of hydroxide ions will be exactly equal to the total number of polymer bound positive charge centers. The concentration of the hydroxide ions in the solution can be found from the following equation:

$$14 - pH = -\log_{10}[OH]$$

The above equation is typically unreliable for all but the most dilute solutions (≤ $2x10^{-3}$ M) [88]. However, polymer samples with a dry mass of 1g or less in a 220mL or greater volume bath is typically dilute enough for the above equation to hold true. Once the concentration of hydroxide anions is calculated, the volume of the 3M KCl bath can then be used to calculate the exact moles of hydroxide anions present in the bath. The last step in the calculation is to divide the moles of hydroxide anions by the dry mass of the polymer sample. This final result will be the ion exchange capacity of the ionomer. The dry mass of the polymer samples can be found by leaving the samples in a vacuum oven set to maximum vacuum and 50°C for 24 hours.

3.6 Measurement of the Water Retention Capacity

The water retention capacity (WRC) is a measure of how much water the polymer can absorb at various relative humidity including the fully hydrated state. This measurement has the dimensionless units of grams of water per grams of dry polymer. The measurement of the water retention capacity is very straight forward. The polymer is first allowed to sit in a controlled humidity chamber for at least 48 hours. After the exposure time has passed, the mass of the polymer is taken using a Mettler Toledo XS105 DualRange analytical balance with 0.01mg accuracy. The sample is then subjected to another environmental condition such as higher or lower relative humidity. For measuring the fully hydrated state, the polymer is allowed to soak in ultrapure Millipore water for at least 48 hours. After the exposure time, the polymer sample is quickly wiped dry of excess surface water with a clean laboratory-grade tissue wipe and its mass is measured. Once the mass of the polymer sample has been taken at all desired environmental

conditions, the dry weight of the sample must be obtained. This is done by allowing the sample to sit in a vacuum chamber set to maximum vacuum for at least 48 hours. After the exposure time, the mass of the dry polymer sample is measured. This mass will be used to find the water retention capacity with the following formula:

$$WRC = \frac{Mass_{wet} - Mass_{dry}}{Mass_{dry}} x100\%$$

3.7 Measurement of the Swelling Ratios

The swelling ratio (SR) is a measure of the expansion of a polymer sample caused by water uptake. In this work, circular samples were used for testing. Each sample was punched from a drop-cast sheet of polymer membrane, which had been soaking in ultrapure Millipore water, using an 18mm diameter circular punch. The diameter and thickness of the samples were then measured as a function of relative humidity. The diameter of the polymer samples was measured with a Mitutoyo caliper with +/-0.01mm accuracy while the thickness of the polymer samples was measured with a Mitutoyo micrometer with +/-0.001mm accuracy. Each sample was allowed to sit in a controlled humidity chamber for at least 48 hours prior to measurement in order to achieve equilibrium. The swelling ratio has the dimensionless units of mm/mm where the expanded wet sample is compared to its smaller dry form. All samples were dried completely by letting them sit in a vacuum chamber at maximum vacuum for at least 48 hours. Once the dry measurements were obtained, the diameter and thickness swelling ratios was calculated with the following formulas:

$$SR_{Diameter} = \frac{Diameter_{wet} - Diameter_{dry}}{Diameter_{dry}} x100\%$$

$$SR_{Thickness} = \frac{Thickness_{wet} - Thickness_{dry}}{Thickness_{dry}} x100\%$$

3.8 Measurement of the Pore Size and Pin Holes

Pin holes are a concern in ionomers since they can cause an electrical short between the cathode and anode. A pin hole is basically a continuous channel that stretches from one side of the membrane to the other. Pin holes are usually created unintentionally when a membrane is cast from a solution and an air bubble becomes trapped during the drying of the membrane. The pore size is the average diameter of a pore that maybe present in the material.

In this work, the average pore size could not be determined directly. However, using a bubble point tester and SEM images, an upper bound on pore size was determined. A Carl Zeiss, SteREO Discovery.V8, modular microscope with 8x magnification was used to check for macroscopic defects such as cracks and pin holes in polymer samples. Additionally, SEM images were used to show any microscopic physical defects as well as the level of porosity in the micrometer range. This data will give an overall impression about the number of defects that are formed when membranes are manufactured using solution casting processes.

The bubble point tester used in this work is a Porous Materials Inc., Bubble Point Tester. A testing sample was prepared by punching out a 16mm diameter disk from a drop-cast membrane. The disk is then checked under a microscope at 8x magnification to ensure that it does not contain any macroscopic defects. Afterwards, the sample was dried in a vacuum oven for 24 hours to remove any water it may have absorbed. The sample is then allowed to

soak in Galwick trademark wetting fluid for a full 24 hours prior to testing. A wetting fluid such as Galwick is required for an accurate test using the bubble point tester since its principle of operation is capillary flow porometry. The wetting fluid will spontaneously fill up any pores within a polymer sample and cannot come back out. The surface free energy of the wetting fluid will be lower than the surface free energy of a sample with a non-reacting gas [61]. The wetting fluid is forced out of the polymer sample by pressurizing one side with an inert gas such as nitrogen. As wetting fluid is forced out of the sample, the inert gas will begin to flow. The machine will then measure the pressure differential across the polymer sample and the gas flow rate. With this information, the largest pore diameter is calculated. The force required to displace the wetting fluid from within the pores is given by the following relationship [61, 89]:

$$p = \frac{4\gamma \cos(\theta)}{D}$$

Where p is the pressure differential across the membrane, γ is the surface tension of the wetting fluid, θ is the contact angle, and D is the diameter of the largest pore in the sample. The contact angle for small surface tension wetting fluids such as Galwick can be assumed to be 0 [61, 90]. The surface tension of Galwick is 16 mJ/m^2.

The pressure of nitrogen gas used in this experiment was set to a maximum of 200 PSI. All calculations and measurements were performed by the included software package. According to PMI, the accuracy of the Bubble Point Tester is 0.15% of the reading with a pore size range of 0.03 – 500 microns. All SEM images were performed by an outside laboratory.

3.9 Measurement of the Glass Transition Temperature

The glass transition temperature is a temperature at which a polymeric material goes form a brittle-like state into a ductile-like state. Although, the physical properties of a material might change drastically during the glass transition, the actual transition is not a phase transition of any kind. It is merely an observed phenomenon that occurs over a range of temperatures.

In this work, the glass transition of the ionomer was measured using differential scanning calorimetry (DSC). The equipment used is a Perkin Elmer DSC6000 with Perkin Elmer aluminum sample pans. 4mm diameter samples were punched out from a sheet of fully hydrated ionomer and then allowed to dry in a vacuum chamber set to maximum vacuum for at least 48 hours. The samples were heated in the DSC from room temperature to 400°C at a rate of 10°C/min under nitrogen gas flowing at 19.8 liters/min. Data was plotted and analyzed in the Perkin Elmer Pyris software. The half-width technique was used to calculate the glass transition temperature of the polymer samples.

3.10 Measurement of the Ionic Conductivity vs. Free Salt Content

One method of improving the ionic conductivity of the ionomer is to add a hygroscopic free salt to the ionomer. The free salt will help improve the ionic conductivity of the ionomer by providing excess free ions and increased water retention. The free ions present in the solid polymer coupled with the increased water content will facilitate charge transfer and thus increase the ionic conductivity. This work investigated the ionic conductivity of the ionomer as a function of the free salt content.

The free salt used in this work was a 50/50 molar mixture of tetramethylammonium carbonate and tetramethylammonium hydroxide. This salt

mixture was chosen because of its compatibility with the ionomer, compatibility with the zinc chemistry, and its hygroscopic properties. Polymer membranes are made by dissolving quaternized polysulfone in the hydroxide form into methanol and concentrated to 15 weight percent. Only the hydroxide form of the ionomer can be used in this experiment because the chloride form of the polymer is not soluble in methanol. Additionally, an aqueous salt solution cannot be added to a DMF chloride polymer solution because the water added will readily anti-solve the chloride polymer out of solution. Due to this complexity, only the hydroxide form of the polymer was studied. In addition, the hydroxide form of the ionomer is the most compatible form with the zinc-air battery and therefore will receive the most attention.

To prepare polymer samples for testing, an aqueous free salt solution is added to the methanol polymer solution in different quantities so that its molar concentration in the ionomer is varied from 0% to 100%. However, it was found that the free salt present in the ionomer causes the drop-cast membranes to crack. The cracking increases with increased salt content. To combat this, polyvinyl alcohol (PVA) polymer is added to the mixture to form a 50/50 molar mixture with the ionomer. In other words, 50% of the total polymer moles in the drop-cast membrane come from the PVA and the other 50% come from the quaternized polysulfone. The PVA forms a more elastic polymer blend that prevents cracking in the ionomer membranes. Once the PVA is added to the polymer solution, test samples are prepared by drop casting them onto pre-cut glass strips that serve as a substrate. The samples are allowed to dry for 24 hours in air at room temperature. Ambient conditions are typically 27°C and 50% relative humidity.

Once test samples are dry, they are installed into the conductivity cell and connected to the Garmy Reference 3000 potentiostat. The cell is placed into a humidity chamber set to 50% relative humidity and allowed to acclimate for 1 hour prior to any testing. The purpose of the acclimation period is to ensure that water transportation into and out of the polymer sample has achieved a steady state. Once acclimation has been achieved, the ionic conductivity of the membrane is found by the procedure described previously. All measurements were performed at room temperature.

This work investigated the ionic conductivity of the following polymer mixtures: pure quaternized polysulfone (QPSU) in the hydroxide form, quaternized polysulfone with PVA and no free salt, QPSU-PVA with 20% free salt, QPSU-PVA with 40% free salt, QPSU-PVA with 60% free salt, QPSU-PVA with 80% free salt, and pure aqueous free salt solution. All percentages are based off of total moles present in the sample not including PVA moles. For example, if a sample were to contain 80% free salt, then 80% of the total moles present would be free salt molecules while the other 20% of the total moles present would be QPSU molecules. A total of 3 samples were tested for each composition listed previously and the average conductivity of those three samples was plotted against the free salt content.

3.11 Measurement of the Concentration and Diffusivity of Oxygen within the Ionomer

The concentration and diffusivity of oxygen in the ionomer was measured by utilizing a combination of hydrodynamic voltammetry and chronocoulometry. This work made use of a Pine Instruments Modulated Speed Rotator and CE Mark equipment along with supporting accessories which include a rotating disk

electrode assembly and polished platinum disk. The rotator was used in a closed system with a special Teflon cell and lid. The shaft of the rotator was modified so that an industrial circular bearing could be installed horizontally. This circular bearing fits the main opening of the cell lid to form a tight seal while allowing the rotator to spin freely. The lid also included four other ports which were used to install a salt bridge for the Hg/HgO reference electrode, the platinum wire counter electrode, an oxygen inlet tube, and an oxygen exhaust tube. All four ports made tight seals with their installed devices to minimize the entry of exterior air. The oxygen inlet was furbished with a pre-bubbler that humidified the incoming oxygen gas. This was necessary in order to control the internal temperature of the electrolyte and proved to yield more consistent results. The exhaust was also furbished with a post-bubbler filled with silicone oil. The purpose of the post bubbler was to minimize exterior air from entering the closed system and to verify that oxygen gas was leaving the system from the intended exhaust. The flow of oxygen was controlled with an external Swagelok T-valve.

Prior to experimentation, the platinum disk was polished for 30 minutes using 1μm Buehler liquid polish followed by polishing for 10 minutes using 0.05μm Buehler liquid polish. After polishing, the platinum disk was thoroughly rinsed under distilled water at high pressure to remove any excess polishing material. Lastly, the platinum disk was heated until glowing red hot in a hydrogen flame. The platinum disk was only polished once for the entire series of experiments, however, the disk was thoroughly rinsed with distilled water followed by flame annealing in the hydrogen flame before each and every experiment.

The first step in this series of experiments is to determine the concentration and diffusivity of oxygen in the electrolyte, i.e. oxygen saturated 0.1M potassium hydroxide, and compare the results to literature values. This step is important for validation of the experimental procedures and equipment. Oxygen was first bubbled continuously into the electrolyte for 1 hour in order to saturate the electrolyte. After saturation, a cyclic voltammetry experiment was performed at numerous rotation rates. The rotation rates (w) used in this work were 100, 400, 900, 1600, and 2500 RPM. The potential was swept from -1V to 0.6V versus a Hg/HgO reference electrode at a scan rate of 10mV/s. The mass-transfer limiting current for oxygen reduction at various rotation rates in the cyclic voltammogram, i.e. the Levich current (i_L), is used to make a Koutecky-Levich plot by plotting $\frac{1}{i_L}\ vs\ w^{-\frac{1}{2}}$. A plot of the data in this fashion will yield a straight line that is characterized by the following equation [91]:

$$\frac{1}{i} = \frac{1}{i_K} + \frac{1}{i_L} = \frac{1}{i_K} + \frac{1}{0.62nFAv^{-\frac{1}{6}}D_O^{\frac{2}{3}}C_O w^{\frac{1}{2}}}$$

In the above equation, $\frac{1}{i_K}$ is known as the kinetically limited current and is the current that would flow in the absence of any mass-transfer limitations. In other words, this current is limited purely by the kinetics of electron transfer. The concentration of reactant species at the surface of the electrode is equal to the bulk concentration under kinetically limited conditions. The value n is the number of electrons transferred in the chemical reaction, the value F is Faraday's constant, A is the surface area of the platinum disk electrode (0.196cm^2), the value v is the kinematic viscosity of the electrolyte (8.98 x 10^{-3} cm^2/s), $D_O$and C_O are the diffusivity and concentration of oxygen in the electrolyte respectively. The

slope of a Koutecky-Levich plot will be equal to $\left(0.62nFAv^{-\frac{1}{6}}D_O^{\frac{2}{3}}C_O\right)^{-1}$ while the intercept will be equal to $\frac{1}{i_K}$. It should be noted that the electron transfer kinetics are very fast in the limiting current region, and thus $\frac{1}{i_k} = 0$. In other words, the Koutecky-Levich plot will intercept the origin at potentials that cause mass-transfer limitation. In this work, values for the limiting current where taken at -0.5V versus the Hg/HgO reference electrode.

All parameters are known in the above equation with the exception of $D_O^{\frac{2}{3}}C_O$. However, a similar product of these two variables can be found from a chronocoulometric experiment. A plot of the charge passed (Q) versus $t^{\frac{1}{2}}$, where t is time, will be linear if the time scale is short [54]. In this system, the time scale is from 0 to 200 milliseconds. Data begins to deviate from linearity after 200 milliseconds. The integrated form of the Cottrell equation characterizes this linear relationship and such a plot is commonly known as an Anson plot. The following is the integrated form of the Cottrell equation:

$$Q = \frac{2nFAD_O^{\frac{1}{2}}C_O t^{\frac{1}{2}}}{\pi^{\frac{1}{2}}}$$

All variables in the above equation represent the same parameters in the Levich equation. The slope of the Anson plot can be used to calculate the product $D_O^{\frac{1}{2}}C_O$ and coupled with the product given by the Koutecky-Levich plot, the diffusivity and concentration of oxygen in the electrolyte can be solved for. A potential of -0.5V versus Hg/HgO was applied for 5 seconds in all chronocoulometry experiments.

The same procedure was used to find the diffusivity and concentration of oxygen in the ionomer once it was verified that these experimental procedures yielded results close to literature values. Finding these values required casting a thin polymer film (ca. 5 - 25μm) directly onto the cleaned platinum disk electrode. This was done by preparing a very dilute casting solution as previously described. It was found that optimal results were obtained from solutions concentrated at 1 - 0.5 weight percent. Films were cast by placing a single drop on the surface of the disk electrode. This drop was carefully spread to the edges of the electrode to ensure a complete coverage of the effective surface area on the platinum disk. The film was allowed to dry in air for a minimum of 24 hours before experimentation. The quality of the polymer film was inspected by an optical microscope at 8x magnification.

Once the polymer film passed inspection, the platinum disk was installed into the rotator. The electrolyte used in these experiments is also 0.1M KOH. Oxygen was bubbled directly into the solution for at least one hour prior to experimentation to ensure oxygen saturation of the electrolyte. As previously described, cyclic voltammetric and chronocoulometric experiments were performed exactly in the same manner as was done for bare platinum with the exception of the scan window and scan rate in the cyclic voltammetric experiment. The potential was swept from -0.495V to -0.505V versus Hg/HgO at a scan rate of 0.1mV/s. This scan window and scan rate yielded the best results.

A Koutecky-Levich plot generated from data of the film covered electrode will also be linear. The current for oxygen reduction in the mass-transfer limiting region is now described by [92]:

$$\frac{1}{i} = \frac{1}{i_L} + \frac{1}{i_F} = \frac{1}{i_L} + \frac{\delta}{nFAD_{O,f}C_{O,f}}$$

The term $\frac{1}{i_K}$ is not included in the above equation since the system is operating in the limiting current region where $\frac{1}{i_K} = 0$. The term $\frac{1}{i_F}$ is the reactant diffusion current and is the current caused by diffusion of oxygen in the polymer film. The term δ is the thickness of the film on the platinum electrode and the terms $D_{O,f}$ and $C_{O,f}$ are the diffusivity and concentration of oxygen in the polymer film respectively. The Levich current term $\frac{1}{i_L}$ remains the same as before. As a consequence, the slope of a Koutecky-Levich plot generated for a film covered electrode will be equal to the slope of a plot generated for a bare electrode. The slope remains the same because it is dependant only on the electrolyte solution [92]. Lastly, the thickness of the film is measured with a Mitutoyo micrometer (+/- 0.001mm) and the product $D_{O,f}C_{O,f}$ is calculated directly from the intercept of the Koutecky-Levich plot.

A chronocoulometric experiment is performed after the cyclic voltammetry experiment. The experiment remains the same as in the case of a bare platinum electrode. The integrated form of the Cottrell equation that was previously presented is also valid for the case of a film covered electrode with the exception that the oxygen diffusivity and concentration terms now reflect mass transport in the polymer film. The product $D_O^{\frac{1}{2}}C_O$ can then be calculated using the slope of the Anson plot generated for the film covered electrode. Lastly, the concentration and diffusivity of oxygen in the ionomer can be calculated using both products obtained from the two experiments. These measurements were performed several times to ensure that data was repeatable.

After experimentation, the thin polymer film is removed from the platinum disk by soaking in a large methanol bath overnight. Methanol will dissolve the hydroxide form of the ionomer. After the methanol bath, the platinum disk is thoroughly rinsed in ultrapure Millipore water and then flame annealed until glowing red hot. This will ensure that the surface of the platinum disk electrode is left clean and ready for further experimentation.

CHAPTER 4

RESULTS AND DISCUSSION

4.1 Ionic Conductivity

The author of this work is primarily interested in studying the hydroxide form of the ionomer since this is the counter anion that is most compatible with the zinc-air battery. However, ionic conductivity measurements of the chloride form of the ionomer were included in this work for intellectual curiosity and comparison. Measurements of both counter anions were made under ultrapure Millipore water. Polymer samples were produced using a die punch that creates samples measuring 30mm x 5mm. The thickness of the sample is the only dimension that varied from sample to sample and was measured using a Mitutoyo micrometer with +/-0.001mm accuracy. The ionic resistance of the membrane was found from the right side semi-circle intersection of the Nyquist plot with the x-axis. Figure 8 below is an example of a typical Nyquist plot:

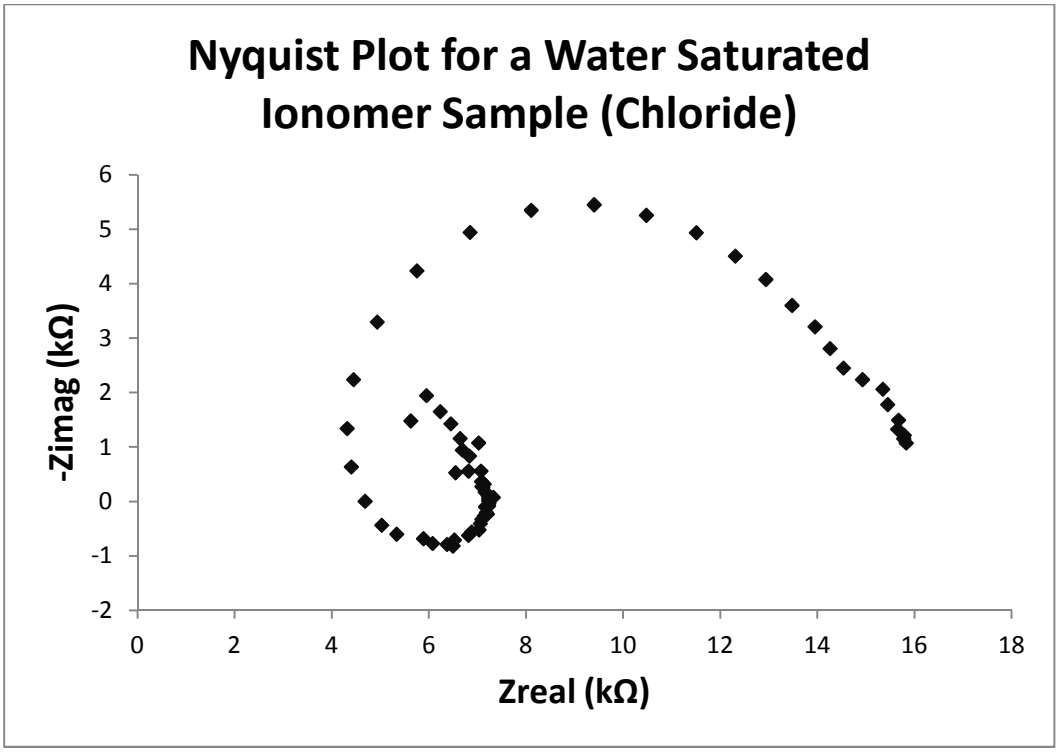

Figure 8. A typical Nyquist plot used to calculate ionic conductivity. The ionomer sample is in the chloride form and is fully water saturated. PEIS with frequency range of 300,000Hz – 0.1Hz.

The ionic conductivity of membrane samples can be readily calculated by measuring the thickness of the membrane and its ionic resistance. The table below summarizes the findings:

Table 2. Ionic conductivity of 5 samples of both counter anions. The average of 5 samples for each counter anion is also shown.

Counter Anion	Ionic Conductivity (mS/cm)	Average (mS/cm)
Hydroxide	41.08	
Hydroxide	39.25	
Hydroxide	37.46	39.92
Hydroxide	40.54	
Hydroxide	41.27	
Chloride	11.45	
Chloride	12.36	
Chloride	11.80	11.80
Chloride	11.25	
Chloride	12.14	

One source of variation in the above results is caused by the conductivity cell. The top half of the cell is clamped to the bottom half with 4 thumb screws. The pressure applied to the polymer sample may vary from measurement to measurement and full contact may not be achieved. Additionally, it is possible to over clamp the specimen and cause physical damage to it that will affect results. The researcher made sure to follow an algorithm in cell assembly in order to guarantee as much consistency as possible, however it is likely that this variation in clamping pressure is reflected in the variation shown in table 2. It can be seen that the hydroxide counter anion is a little more than 3 times as conductive as the chloride counter anion under fully hydrated conditions. One possible explanation for this observation is that the hydroxide anion is smaller, and therefore more mobile, than the chloride counter anion. The hydroxide anion has an effective ionic radius of 153 picometers [93] while the chloride anion has an effective ionic radius of 181 picometers [94]. Another explanation is that the hydroxide anion is a polarized heteronuclear diatomic molecule with the oxygen atom having a full negative charge and the hydrogen atom having a partial positive charge [95].

This hydrogen atom can cause partial shielding from the polymer-bound positive charge centers. In contrast, the chloride anion is a single negatively charged atom with high electronegativity. Lastly, the hydroxide anion can quickly convert back and forth between a neutral water molecule and a charged diatomic molecule due to the self-ionization of water [88, 96]. This rapid transfer of protons between molecules would give the hydroxide anion higher ionic mobility than the chloride anion.

The above results indicate that the hydroxide form of the ionomer is better suited for the zinc-air battery from the point of view of maximizing the ionic conductivity. This is a good result since only the hydroxide form the ionomer is actually compatible with the chemistry of the zinc-air battery.

4.2 Ion Exchange Capacity

The ion exchange capacity (IEC) is a measure of the number of polymer-bound positive charge centers. This is an important chemical property that gives insight to the degree of quaternization and the effectiveness of the polymer to function as an electrolyte. The theoretical ion exchange capacity, assuming 100% degree of quaternization, can be calculated directly from the degree of chloromethylation of the chloromethylated polymer. In fact, the theoretical molecular weight of the quaternized polysulfone used in this work is calculated in the same way the molecular weight of chloromethyl polysulfone is calculated. If the quaternization reaction were to proceed to 100% completion, then 114% quaternized polysulfone would have the following molecular weight:

$$114\%\ QPSU = (0.14) * \left(692.90 \frac{g}{mol}\right) + (0.86) * \left(567.71 \frac{g}{mol}\right) = 585.24 \frac{g}{mol}$$

In addition, for every mole of polysulfone monomers, there will be 1.14 times more tertiary amine substituent groups, i.e. polymer-bound positive charge

centers. With this information, the theoretical ion exchange capacity can be calculated assuming a 1 gram basis:

$$mmol\ tertiary\ amine\ in\ 1g = \frac{1g}{585.24\frac{g}{mol}} * 1.14 * 1000\frac{mmol}{mol} = 1.948\ mmol$$

There are 1.948 millimoles of tertiary amine groups in one gram of ionomer. Therefore the theoretical ion exchange capacity is:

$$IEC_{Theoretical} = 1.948\frac{mmol}{g}$$

Below are the results from three independent samples measured twice each.

Table 3. Results from the IEC measurements showing the average for each sample and a grand average of all measurements. Units are mmol/g.

Sample	IEC1	IEC2	Average	Grand Average
1	0.997	0.974	0.986	
2	1.069	1.021	1.045	1.022
3	1.070	0.999	1.035	

The table above shows the results for all 6 measurements, 2 measurements for each sample. In addition, the table shows the average of two measurements for each sample and the average of all 6 measurements known as the grand average. If the grand average is compared to the theoretical IEC, then it can be seen that the grand average is about half the magnitude of the theoretical value. This is an indication that not all chloromethyl groups are being converted into tertiary amine groups in the quaternization reaction.

The author of this work does not precisely know the explanation for this observation. However, the author speculates that the operating conditions of the quaternization reaction are not ideal and could be further improved. This work did not investigate the optimal operating conditions for the quaternization reaction

but would certainly be a point of interest for future work. It is speculated that adjusting the reaction temperature, reaction time, and molar ratios of the chemical reagents could improve the reaction conversion and therefore increase the IEC of the ionomer.

It can be seen from table 3 above that the IEC of all three samples decreased in the second IEC measurement. The exact cause of this observation is not known. However, a difference in temperature of 3M KCl bath at the time of measurement could be the cause for the decrease in IEC. All pH measurements were made with a ThermoScientifc Orion 4 Star electronic pH meter. These pH measurements are temperature sensitive and thus the instrumentation is calibrated prior to the measurement to minimize the effect of day to day temperature differences. Since the measurements for the second run were conducted several days after the first run, it is possible that a difference in room temperature caused the values of the second measurement to be less than the first even though the equipment was calibrated prior to the measurement for both runs. Apart from error in the instrumentation, the author could not come up with another explanation for the slight decrease in IEC in the second run of measurements.

4.3 Water Retention Capacity

The maximum water retention capacity (WRC) was measured for both the chloride and hydroxide form of the ionomer. Additionally the water retention capacity as a function of relative humidity has also been reported for both forms of the polymer. Table 4 below shows the maximum water retention capacity.

Table 4. Maximum water retention capacity for the chloride and hydroxide form of the polymer.

Counter Anion	WRC	Average
Hydroxide	1.762	
Hydroxide	1.715	
Hydroxide	1.733	1.726
Hydroxide	1.721	
Hydroxide	1.700	
Chloride	0.667	
Chloride	0.699	
Chloride	0.697	0.679
Chloride	0.699	
Chloride	0.634	

It should be noted that the values in table 4 above would need to be multiplied by 100 to get their percent water retention capacity. For example, the hydroxide form the ionomer has an average WRC of 172.6%. This indicates that the hydroxide form of the ionomer would absorb 172.6% of its dry mass in water. Comparing the hydroxide form to the chloride form, we can see that the hydroxide form of the ionomer has a maximum WRC that is more than twice as great as the chloride form. This result indicates that the hydroxide form of the ionomer is better suited for the zinc-air battery since water is required for the chemistry to work. Having more water in the ionomer will increase the ionic conductivity until it reaches its maximum. The greater the ionic conductivity, the better the battery performance will be.

Figure 9 below shows the water retention capacity for 3 samples of the hydroxide form and 3 samples of the chloride form of the ionomer as a function of relative humidity. The reader should note that 100% relative humidity indicates that the sample has been equilibrated with a distilled water bath.

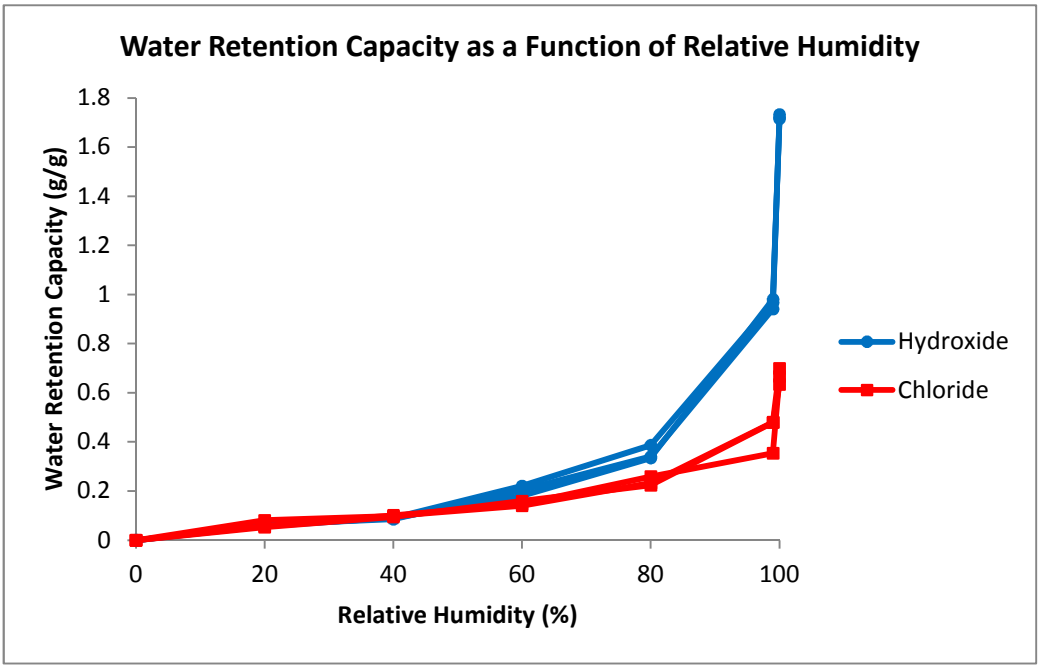

Figure 9. Water retention capacity for the hydroxide and chloride form of the ionomer as a function of relative humidity.

Figure 9 shows that the WRC for both the chloride and hydroxide forms of the ionomer remain roughly the same up until 40% relative humidity. We start to see a divergence in the curves around 50% relative humidity and they become significantly different at 60% relative humidity. From there on out, the hydroxide form of the ionomer clearly shows that it can store more water than the chloride form at any given relative humidity. Additionally, the plot shows that the rate of change in WRC increases more rapidly after 80% relative humidity for both forms of the polymer. In fact, the WRC nearly doubles for the hydroxide form of the ionomer when the relative humidity is increased from 99% to 100%. The WRC of the chloride form of the ionomer increases by 50% - 75% when the relative humidity is increased from 99% to 100%.

Lastly the author would like to point out that one of the data points for a chloride sample at 99% relative humidity in figure 9 is lower than the other two

points. The author of this work could not find an explanation for this low value but speculates that there was an error in the measurement of its mass. After further investigation, the author concludes that this data point is an outlier and should not be taken seriously.

4.4 Swelling Ratios

The swelling ratio is a measure of the expansion of the ionomer when it absorbs water. In this experiment, the expansion of circular disks was tracked by measuring their diameters and thicknesses. In addition to finding the maximum swelling ratio under fully humidified conditions, the swelling ratio as a function of relative humidity was also reported. The samples used for this experiment where punched out from a single sheet of ionomer prepared with the drop cast method. Each sample had a fully hydrated diameter of 18mm. Table 5 and 6 below show the maximum diameter and thickness swelling ratios for 5 hydroxide and chloride form samples.

Table 5. The maximum swelling ratio for the diameter and thickness of 5 hydroxide form circular samples.

Hydroxide	Sample 1	Sample 2	Sample 3	Sample 4	Sample 5	Average
$SR_{Diameter}$	0.33	0.37	0.33	0.34	0.35	0.34
$SR_{Thickness}$	0.59	0.49	0.59	0.59	0.51	0.55

Table 6. The maximum swelling ratio for the diameter and thickness of 5 chloride form circular samples.

Chloride	Sample 1	Sample 2	Sample 3	Sample 4	Sample 5	Average
$SR_{Diameter}$	0.32	0.33	0.32	0.32	0.32	0.32
$SR_{Thickness}$	0.21	0.31	0.30	0.31	0.29	0.28

The above data is important information for battery cell design since expansion of the ionomer due to water absorption will need to be accounted for.

Table 5 indicates that a round, hydroxide form, electrolyte membrane may expand up to 34% in its diameter and 55% in its thickness while the chloride form may expand up to 32% in its diameter and 28% in its thickness as seen in table 6. It should be noted that hydroxide form samples 2 and 5 have thickness swelling ratios that are low compared to samples 1, 3, and 4. Additionally, chloride form sample 1 has a thickness swelling ratio that is smaller than the rest of the samples in the group. These inconsistencies are most likely caused by error in the thickness measurements. Samples tend to wrinkle as they shrink and most likely cause more error in the thickness measurements than it does in the diameter measurements. It can be seen that diameter swelling ratios are consistent across all samples for both forms of the ionomer. It is interesting to see that the hydroxide form has an average thickness swelling ratio that is larger than the average diameter swelling ratio while the chloride form has diameter and thickness swelling ratios that are very close to each other. Furthermore, the average hydroxide form diameter swelling ratio is only slightly larger than the average for the chloride form. Lastly, the hydroxide form of the ionomer has a thickness swelling ratio that is larger than the chloride's; almost twice as large. These data indicate that lateral expansion for both forms of the ionomer can be expected to be roughly the same. However, the hydroxide form of the ionomer is expected to expand more in its thickness than the chloride form. This is information that will be useful in battery cell design.

Due to the importance that swelling plays in cell design, the swelling ratio as a function of relative humidity has been reported for the hydroxide and chloride form of the polymer. Figure 10 shows the diameter swelling ratio as a function of relative humidity while figure 11 shows the thickness swelling ratio as

a function of relative humidity for three polymer samples of both counter anions. The reader should note that 100% relative humidity implies that the sample is in equilibrium with a distilled water bath and is fully hydrated.

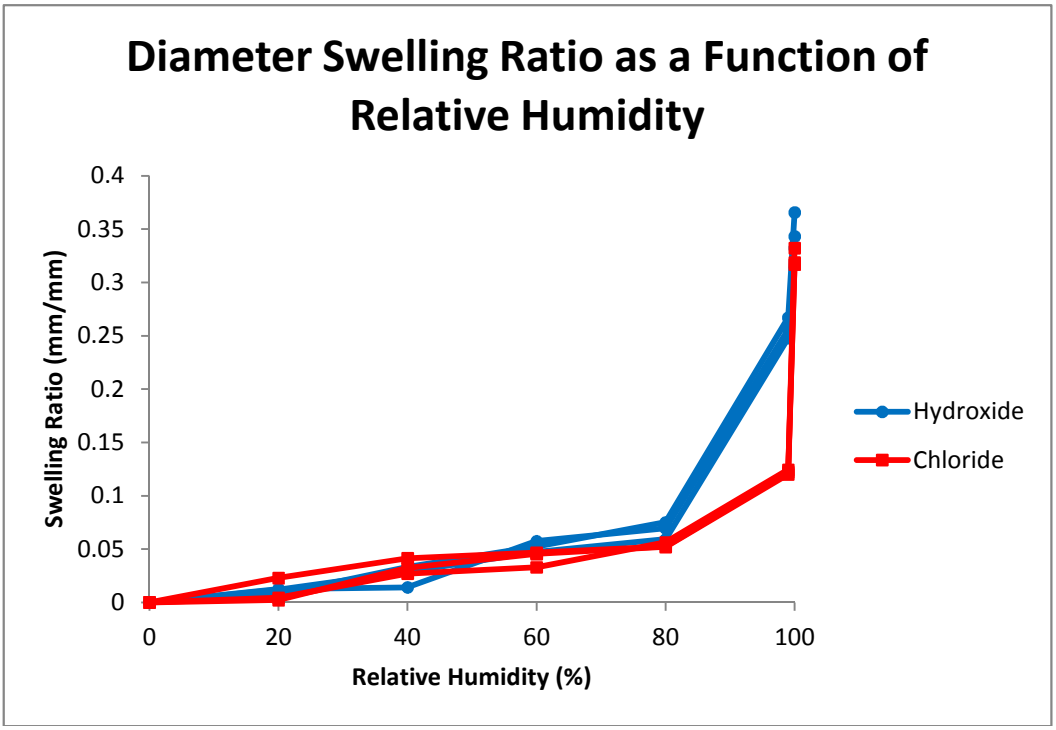

Figure 10. Diameter swelling ratio as a function of relative humidity for three samples of each counter anion.

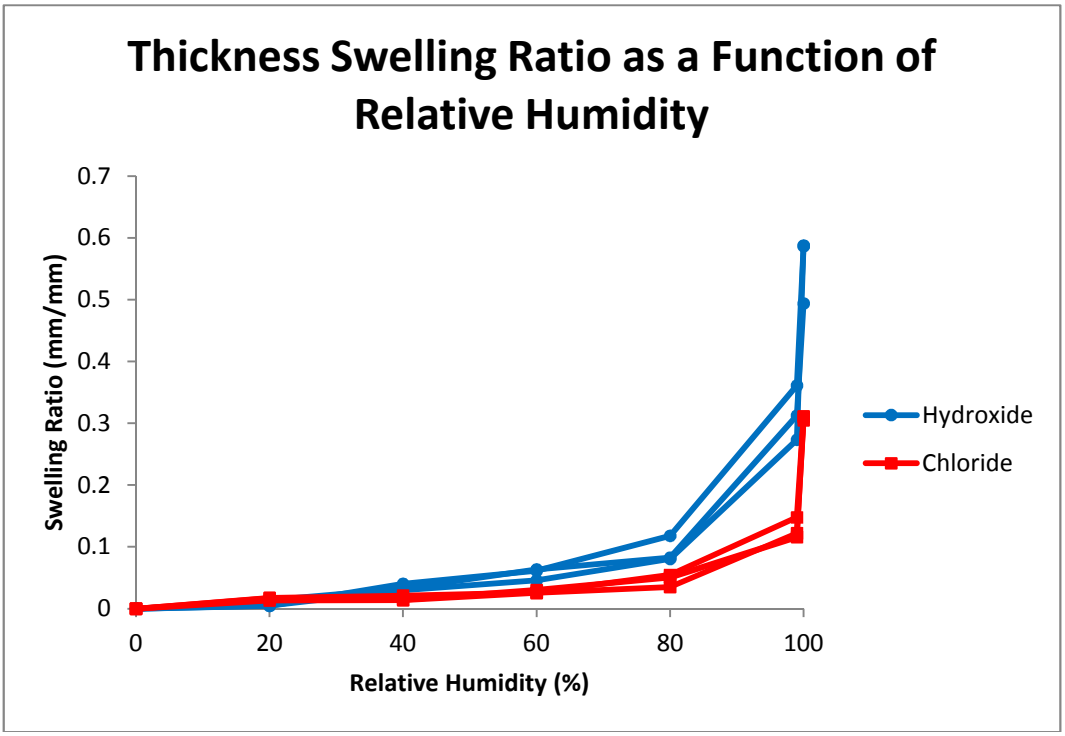

Figure 11. Thickness swelling ratio as a function of relative humidity for three samples of each counter anion.

The data in figure 10 show that the diameter swelling ratio for both forms of the ionomer is more or less the same up until 80% relative humidity. Beyond 80% relative humidity, the hydroxide form of the ionomer has a greater diameter swelling ratio than the chloride form. At 100% relative humidity, the hydroxide form has a diameter swelling ratio only slightly greater than that of the chlorides'. However, at 99% relative humidity, the hydroxide form has a diameter swelling ratio that is much greater than the chlorides'. This is an indication that the hydroxide form of the ionomer will begin to swell more in its diameter than the chloride form as the relative humidity increase from 80%.

We can see some spread amongst groups of data points in the curves for both counter anions in figure 10. This spread in the data is surely caused by experimental error in measurements. The dehydration of the circular polymer

samples causes them to shrink non-uniformly. The samples will still retain a circular shape as they dehydrate in decreasing relative humidity; however, their shape is no longer perfect. To combat this, the diameter of each sample was measured 5 times in different directions and then averaged so that that average value could be used in calculations. Nonetheless, it is clear that experimental error in the measurement is still present in the data. It should be noted though, that this technique did improve the quality of the data as initial attempts were difficult to interpret.

Figure 11 shows a different trend than figure 10. It can be seen that the thickness swelling ratio of the hydroxide form of the ionomer begins to become greater than that of the chlorides' around 40% relative humidity. This data indicates that the expansion of the electrolyte in a zinc-are battery cell will be more pronounced in the hydroxide form than in the chloride form. This is especially true at relative humidity greater than 80%. That observation will be important to note when designing a zinc-air battery cell since the hydroxide form of the ionomer will most likely be used.

The thickness swelling ratio data points for the hydroxide form seem to have more spread at 80%, 99%, and 100% relative humidity than the data points for the chloride form. As stated previously, samples tend to wrinkle as they shrink due to dehydration. The wrinkling was observed to be more pronounced in the hydroxide form than in the chloride form. Therefore, it was expected that error in the measurements for the hydroxide form polymer samples would be greater than the error found in measurements of the chloride form polymer samples. This error causes more spread at higher relative humidity because the calculation of the swelling ratio is based off of the difference in magnitudes of physical

dimensions. Since the difference is greatest at the higher relative humidity, the error will be more pronounced.

Lastly, it is important to note that the shape of the curves in figures 10 and 11 all resemble the shape of the curves in figure 9 (WRC). It can be seen that the water retention capacity and the swelling ratios are very closely related.

4.5 Pore Size and Presence of Pin Holes

The average pore size could not be precisely determined in this work. However, an upper limit to pore size was established with the use of a bubble point tester and SEM images. The largest pore size in a single sample, as determined by the bubble point tester software, was found to be 32.6nm. This result is slightly greater than the machine's smallest detection limit for pore size (30nm), thus it is believed to be credible. However, any other pores present in the sample will be smaller than 32.6nm. The sample did not suffer from any kind of mechanical failure during the testing. A thorough inspection using a microscope set to 8x magnification confirmed this. Only one sample was tested in the bubble point tester because it was found that the sample caused the sample chamber to lock up very tightly. A great deal of effort was needed in opening the sample chamber and the researcher did not want to risk damaging the equipment if subsequent samples were to also cause lockups.

Figure 12 are two SEM images with different magnifications showing the morphology of the polymer sample. The images are focused on a cross-sectional edge of a polymer casting.

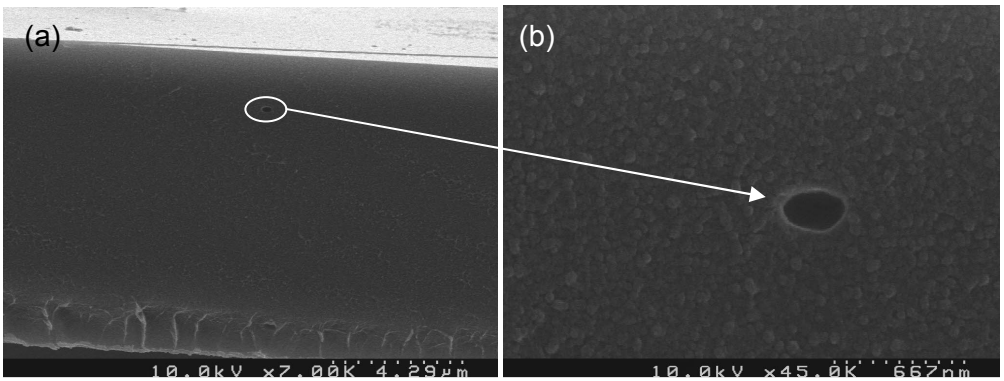

Figure 12. SEM images of a cross section of an ionomer sample. (a) SEM image showing uniformity from top to bottom, 7000x magnification. (b) Close up SEM image of a small cavity shown in Figure 12(a), 45000x magnification.

Figure 12(a) shows that the ionomer is uniform throughout its structure. There are no obvious pin holes or channels going through it. Figure 12(b) shows a close up of a cavity found in figure 12(a). This cavity is ca. 334nm wide and 200nm tall. The cavity is most likely the result of a small air bubble trapped within the material. Each tick mark in the scale bar in figure 12(b) is spaced apart by a distance of 66.7nm. According to the bubble point tester results, the largest pore size found was 32.6nm in diameter which is roughly half the spacing between tick marks. Such a pore is difficult to see in figure 12(b) if there are any present. Actually, it is difficult to estimate the average pore size by inspecting figure 12(b) and it would stand to reason that the average pore size would have to be much smaller than 32.6nm.

As future work, the author would like to acquire SEM images at higher magnification. Furthermore, a mercury intrusion technique could be used to better understand the porosity of the material. Lastly, the author would like to perform X-ray diffraction on a sample of powdered ionomer to investigate its structure and determine if any crystallinity exists.

4.6 Glass Transition Temperature

The glass transition temperature of the ionomer was found using a Perkin Elmer DSC6000 and results were analyzed with the included Pyris software. The temperature was swept from room temperature to 400°C at a rate of 10°C/min under nitrogen gas flowing at 19.8 liters/min. All glass transition temperatures were calculated using the half width technique in the software package. Before experimentation on the ionomer was initiated, the glass transition temperature of polysulfone was first measured to ensure that the equipment was operating properly and experimental procedures were correct. Figure 13 is a plot of typical data for the polysulfone base polymer used in the chloromethylation reaction.

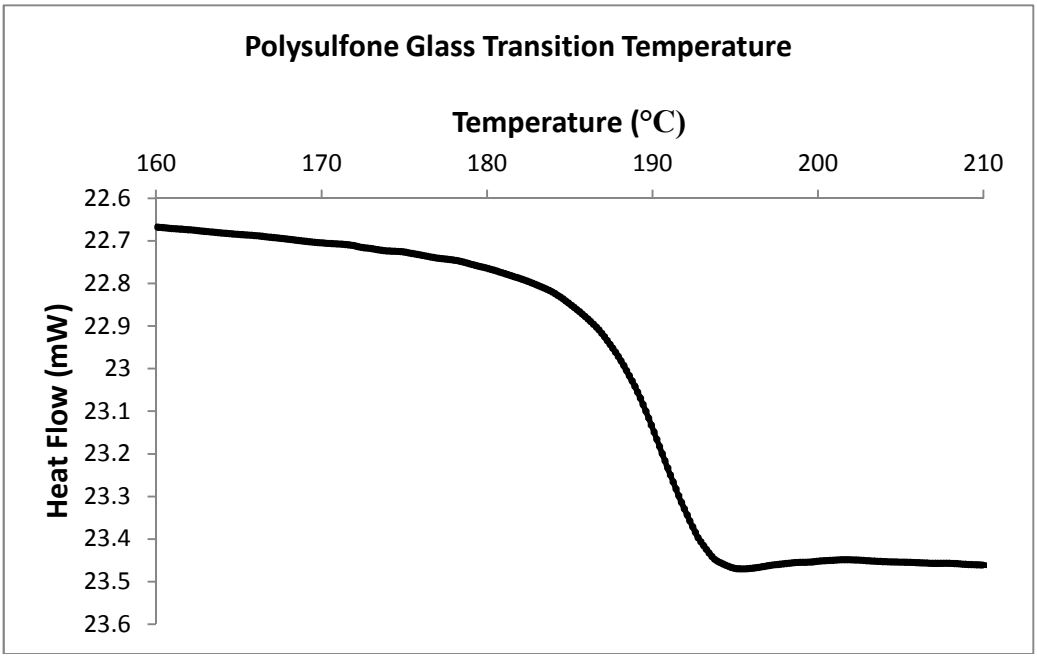

Figure 13. Glass transition temperature data for a polysulfone sample. The glass transition occurs at 198.91°C using the half width calculation.

The glass transition temperature in figure 13 is 189.91°C using the half width calculation on the Pyris software. This measurement was repeated a total

of 3 times and Figure 13 is a typical plot of the results. All three glass transition temperatures measured for 3 different samples of polysulfone were within 2°C of each other. The high glass transition temperature is caused by the aromatic rings in polysulfone. These aromatic rings serve as chain stiffeners and reduce the flexibility of polymer chains. The direct consequence is an increase in the observed glass transition temperature. According to Boedeker Plastics, the glass transition temperature of polysulfone is 190°C [97]. Needless to say, it is safe to assume that the experimental procedures and equipment are adequate for testing.

These same procedures were applied to three samples of the ionomer in the chloride form. Figure 14 is a typical plot of data from this experiment and shows the full temperature range.

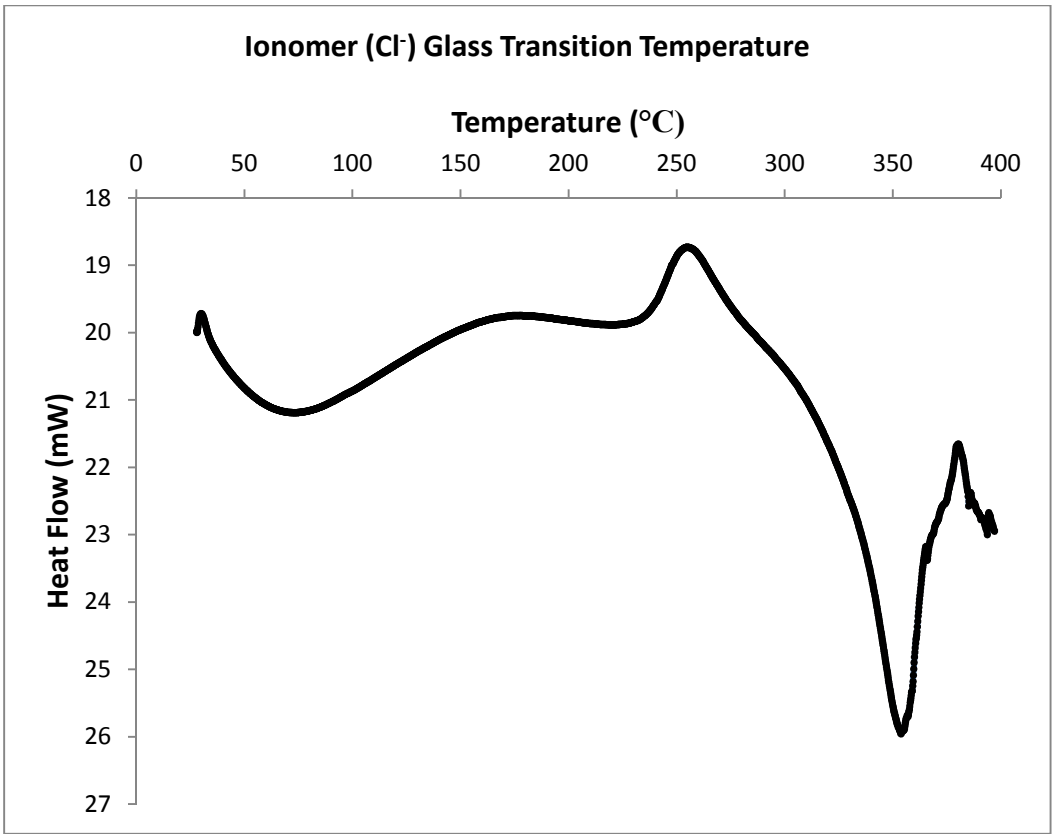

Figure 14. Glass transition temperature data for the ionomer in the chloride form. Glass transition temperature is suspected to occur at 344.01°C using the half width calculation.

Figure 14 shows interesting peaks that could not be explained at the time of writing this document. However, these peaks were present in the data for all three samples of the ionomer. Additionally, the data for all three samples is very similar. The glass transition temperature is believed to be in the steepest portion of the curve in figure 14. The average of all three measurements indicates that the glass transition temperature of the ionomer is 344.53°C. However, is was observed that polymer samples had turned into a dark black color after testing and seemed to have melted on the surface of the aluminum sample pan. The polymer samples could be described as “charred” or “burnt” after testing. This observation would indicate that the samples were chemically degrading at these

high temperatures. Complete chemical degradation would most likely occur at around 350°C and higher. One sample was heated to 325°C and then cooled back to room temperature. This sample did not undergo any changes in its physical shape, but did change from a light yellow color to a dark orange color. This observation would indicate that the sample was starting to degrade at 325°C. Based off of these observations, the author concludes that the glass transition temperature probably coincides with the degradation temperature of the ionomer. The degradation of the ionomer makes it difficult to report the glass transition temperature with certainty and further investigation would be needed to obtain a reliable value. However, the glass transition temperatures of the polysulfone samples and the suspected glass transition temperatures of the ionomer are reported in table 7.

Table 7. Glass transition temperatures for three samples of polysulfone and the ionomer in the chloride form. All glass transitions temperatures were measured using the half width calculation.

Sample	Material	Glass Transition Temperature (°C)
1	Polysulfone	187.65
2	Polysulfone	189.91
3	Polysulfone	189.07
4	Quaternized Polysulfone	344.80
5	Quaternized Polysulfone	344.77
6	Quaternized Polysulfone	344.01

4.7 Ionic Conductivity vs. Free Salt Content

One method of improving the ionic conductivity of the ionomer is to dope the membranes with a hygroscopic salt. The extra ions present in the polymer membrane, along with the additional water absorbed from the air, will improve

ionic mobility. The salt contents of interest in this experiment were 0%, 20%, 40%, 60%, 80%, and 100% by molar amount. 0% free salt indicates that the ionomer is devoid of any free salt while 100% free salt implies that the sample is pure aqueous free salt solution. All samples were equilibrated and tested at 50% relative humidity and 27°C. Three replicates were tested at each concentration and the average ionic conductivity of the three replicates was plotted against the free salt content. Figure 15 is a plot of the results.

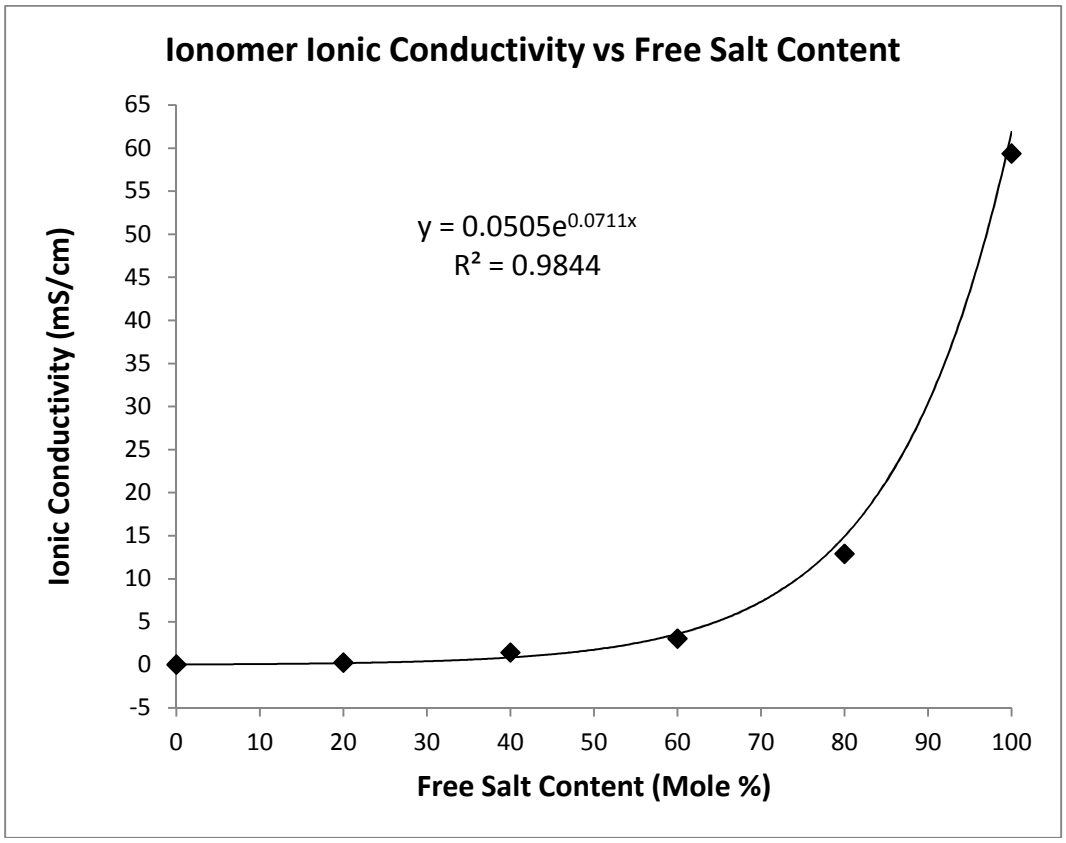

Figure 15. A plot of ionomer ionic conductivity versus free salt content at 50% relative humidity.

An exponential regression was applied to the data points. The R^2 value of 0.9844 indicates that this exponential regression has a very good fit with the data. The maximum averaged ionic conductivity that was achieved by adding

free salt to the ionomer was found to be 12.90mS/cm. This corresponds to the 80% free salt samples. The lowest averaged ionic conductivity that was measured in this test came from the 0% free salt samples. Their averaged ionic conductivity was found to be 0.03mS/cm. The data indicate that every 10% increase in free salt content will roughly double the ionic conductivity. This result indicates that doping the ionomer is indeed advantageous. However, there is a practical limit to how much free salt can be added. The researcher found that membrane samples prepared with 80% free salt tend to tear easily and make manipulation very difficult. For a battery cell application, having 80% free salt content or greater will pose additional challenges in manufacturing. The researcher recommends doping membranes in the range of 40% - 60% free salt. These membranes offered excellent room temperature ionic conductivity along with acceptable workability and toughness.

4.8 Oxygen Concentration and Diffusivity in the Ionomer

The concentration and diffusivity of oxygen in the ionomer was measured electrochemically using a rotating disk electrode. More specifically, cyclic voltammetry and chronocoulometry was used to form Koutecky-Levich and Anson plots respectively. The slopes of these plots were used to calculate the diffusivity and concentration of oxygen in the ionomer. The first step in experimentation, however, was to find the concentration and diffusivity of oxygen in 0.1M KOH solution and compare the experimental values to literature values. Additionally, the Kouteck-Levich data can be compared to theoretical values published in the literature. This step is necessary for proving that the system is working properly and results can be trusted. Figure 16 is a plot of experimental

data plotted against theoretical data for a 4 electron oxygen reduction pathway. Theoretical data was taken from the work presented by Xuguang Li *et al* [51].

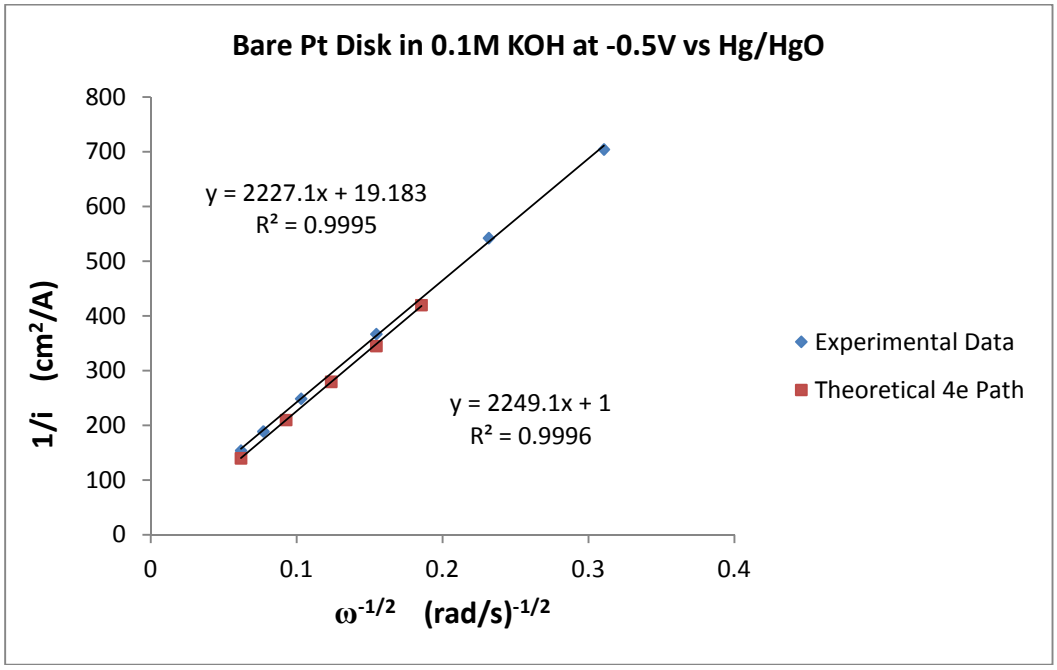

Figure 16. Koutecky-Levich plot of experimental data and theoretical 4 electron oxygen reduction pathway. Scan rate of 10mV/s and limiting currents measured at -0.5V versus Hg/HgO. Solution is oxygen saturated 0.1M KOH. Bare platinum disk electrode.

It can be seen from Figure 16 that the experimental data agrees very closely with the theoretical data. The slopes of the two curves differ by less than 1%. Furthermore, the intercept of the experimental data is very close to 0. This result confirms that oxygen is being reduced via the 4 electron pathway in the cyclic voltammetry experiment to form hydroxide anions.

$$O_2 + 2H_2O + 4e^- \rightarrow 4OH^-$$

The author of this work is not sure why the intercept of the experimental data is not 0, however it is speculated that the discrepancy is caused by experimental error in the equipment.

After the cyclic voltammogram was performed, a chronocoulometric experiment was conducted. Figure 17 is an Anson plot generated from the experimental data.

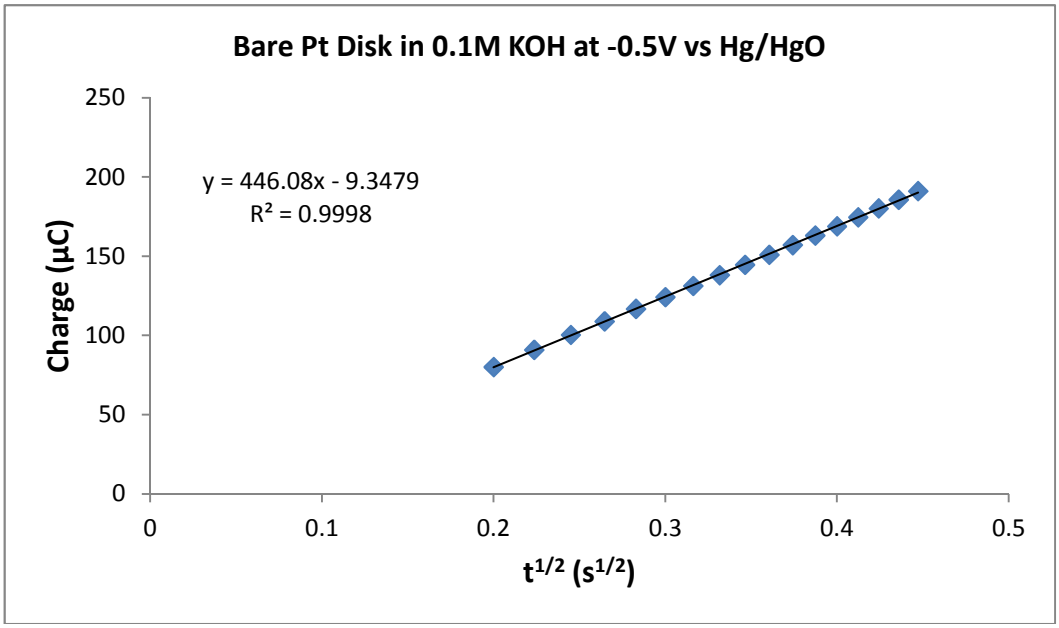

Figure 17. Anson plot of chronocoulometric data using a bare platinum disk electrode. Applied potential of -0.5V vs Hg/HgO in 0.1M KOH.

Figure 17 shows the linear portion of the data in the chronocoulometric experiment within the short time scale. The first 30 milliseconds of data have been truncated since they do not align with the remainder of the curve. It can be seen that the linear regression applied to the data in the Anson plot has a very good fit. The concentration and diffusivity of oxygen in 0.1M KOH was calculated using the slope from the Anson plot and the Koutecky-Levich plot. It was found that the concentration of oxygen in the electrolyte was 1.2×10^{-3} M while the diffusivity of oxygen was found to be 1.9×10^{-5} cm^2/s. These values can be compared to literature values in table 8.

Table 8. Literature values of concentration and diffusivity of oxygen in fully saturated 0.1M KOH solution.

Reference		Concentration $x10^3$ (M)	Diffusivity $x10^5$ (cm^2/s)
D. Zhang *et al*	[53]	1.15	1.95
K. Gubbins *et al*	[58]	1.2	1.9
X. Li *et al*	[51]	1.3	1.7

It is clear that the experimental results match that of literature values and it can therefore be concluded that the experimental apparatus and procedure are adequate for further experimentation.

A total of three film castings were experimented on. Each casting had a different thickness. The castings used in this experiment were 12μm, 16μm, and 25μm thick. Figure 18 is a Koutecky-Levich plot of the data obtained from all three film thicknesses.

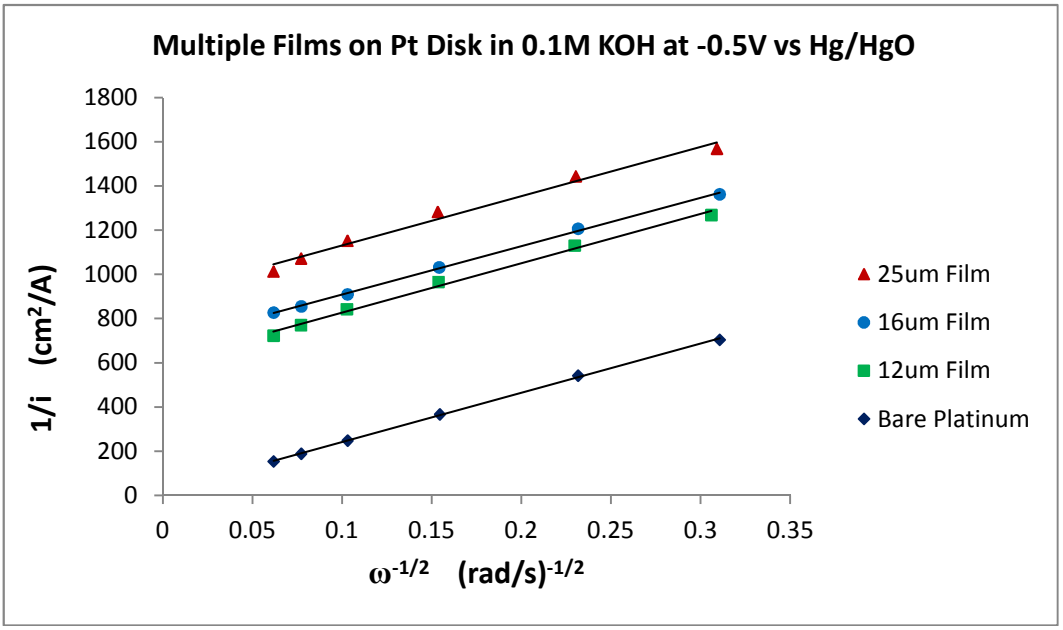

Figure 18. Koutecky-Levich data for 12μm, 16μm, and 25μm thick ionomer films on a platinum disk polarized to -0.5V versus Hg/HgO. Electrolyte is oxygen saturated 0.1M KOH. Bare platinum data is also shown.

The data in figure 18 for all three films are parallel to the data for bare platinum as was predicted by the theory. Additionally the spacing between the curves seems appropriate; the data for the 16μm film lies more closely to the data for the 12μm film than it does to the 25μm film. The intercepts of these data are the key features needed for the calculation of oxygen concentration and diffusivity within the ionomer. Technically, the data from a single polymer film is all that is needed to calculate the concentration and diffusivity of oxygen. However, three films were tested to show the variability of the measurement. The concentration and diffusivity of oxygen was calculated using an averaged slope from the Anson plot. Figure 19 is a typical Anson plot for the polymer films. In theory, all Anson plots should be identical as they do not depend on film thickness. However, it was noticed that the slope of the Anson plots varied from measurement to measurement. Therefore a total of 8 slopes from 8 different Anson plots were averaged so that all concentration and diffusivity calculations could be made using the same Anson slope. The averaged Anson slope was 237 $\mu C\ s^{-1/2}$ with a standard deviation of 10.2 $\mu C\ s^{-1/2}$.

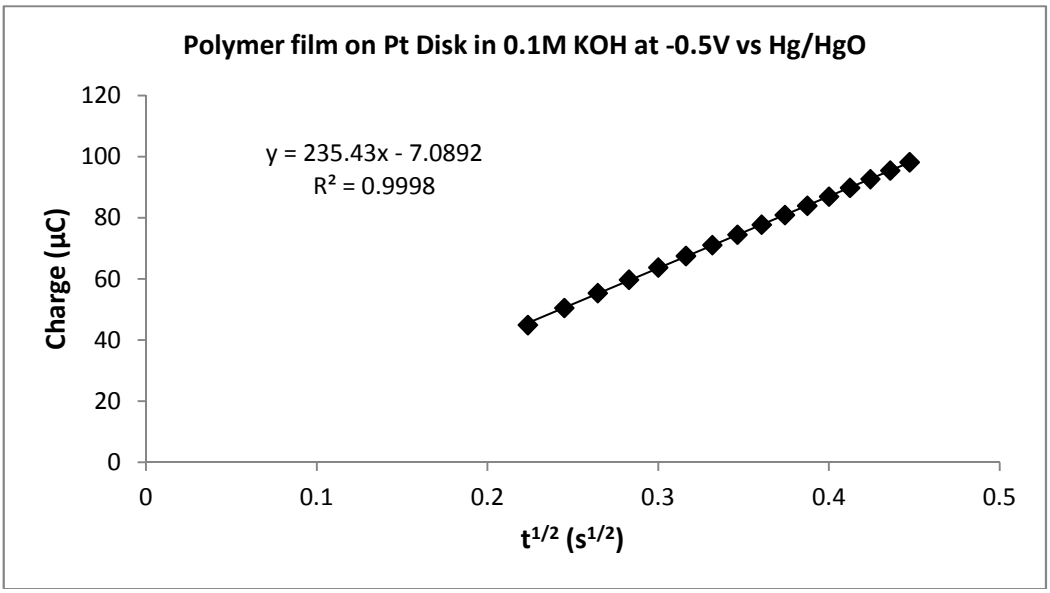

Figure 19. Typical Anson plot of the data from a chronocoulometric experiment. Platinum disk polarized to -0.5V versus Hg/HgO in oxygen saturated 0.1M KOH.

The results of the experiment and the linear regressions for the data presented in figure 19 can be seen in table 9.

Table 9. Oxygen concentration and diffusivity in the ionomer for three film thicknesses. Linear regressions from the Koutecky-Levich plot have been included.

Sample Thickness	Concentration $x10^3$ (M)	Diffusivity $x10^5$ (cm^2/s)	Linear Regression
12µm	1.5	0.35	y = 2231.6x + 907.73
16µm	1.3	0.47	y = 2188.6x + 690.07
25µm	1.1	0.66	y = 2228.8x + 604.43

A particular trend can be seen in the results presented in Table 9. The concentration of oxygen is highest in the thinnest film and lowest in the thickest film. Likewise, the diffusivity of oxygen is highest in the thickest film and lowest in the thinnest film. The theory presented previously indicates that these values should be independent of film thickness, especially if the material is the same for

all castings. Indeed, only one polymer casting solution was used to make film castings. The thickness of the polymer films was controlled by altering the volume of solution added to the platinum disk. It can therefore be concluded that these results have an experimental error factored into them. The author of this work rigorously attempted to identify the source of error but was unable to do so. It is speculated that the system may not be operating at steady state during the measurement because oxygen diffusion is not fast enough to keep up with changes in potential despite the slow scan rate of 0.1mV/s. Further study would be required to confirm this and improve upon the methodology.

The data presented in table 9 will be averaged and a tolerance will be provided due to the observation of this trend. Table 10 summarizes the experimental results for this experiment.

Table 10. Summary of results as calculated from experimental data.

Electrolyte	Concentration $x10^3$ (M)	Diffusivity $x10^5$ (cm^2/s)
0.1M KOH	1.2	1.9
Ionomer	1.3 ± 0.2	0.49 ± 0.15

Table 10 shows that the concentration of oxygen in the ionomer is very close to the concentration of oxygen in the aqueous 0.1M KOH solution. This result makes sense since it was originally expected that the concentration of oxygen in the ionomer would be less than, or at the very most, not much greater than the concentration of oxygen in the aqueous electrolyte. It is possible that the concentration of oxygen in the ionomer is actually greater than the concentration of oxygen in the aqueous electrolyte do to the tolerance level of the measurement. However the difference between the two would be small as

expected. It can be seen from table 10 that the diffusivity of oxygen in the ionomer is about 4 times less than the diffusivity of oxygen in the aqueous electrolyte. This result also makes sense and agrees with the researcher's intuition. We can imagine that diffusion in a solid would be much slower than diffusion in a liquid since all molecules are allowed to move more freely in the aqueous system. In contrast, the polymer chains have very limited mobility and have formed a solid structure; movement of the oxygen molecules will be hindered by the rigid polymer chain structure.

CHAPTER 5

CONCLUSIONS AND FUTURE WORK

5.1 Conclusions

5.1.1 Ionic Conductivity Conclusions

The ionic conductivity testing showed that the hydroxide counter ion offered higher ionic conductivity than the chloride counter ion under fully water saturated conditions. This is a positive result since the chloride anion is not compatible with the chemistry of the zinc-air battery and getting as much ionic mobility as possible will help maximize its power density.

5.1.2 Ion Exchange Capacity Conclusions

It was determined that measuring the IEC of the ionomer was a good method of measuring the degree of conversion in the quaternization reaction. The advantage of this technique is that the procedure is simple and requires inexpensive equipment. The most complex component required would be the pH meter. It was shown that the IEC of the ionomer tested in this work was about half the magnitude of the theoretical value which was calculated assuming 100% conversion of the chloromethyl groups. This is an indication that the functionality of the ionomer could be further improved by optimizing the reaction conditions of the quaternization reaction. Additionally, increasing the degree of chloromethylation of the chloromethylated polysulfone used in the quaternization reaction could also lead directly to higher IEC values. The chloromethylation reaction would have to also be optimized for this. Improving the IEC of the ionomer could play a key role in optimizing the performance of a zinc-air battery. Having more polymer-bound positive charge centers per unit volume, or per unit mass, could improve the ionic conductivity of the ionomer. Improved ionic

conductivity may have a positive effect on the power density of the zinc-air battery.

5.1.3 Water Retention Capacity Conclusions

The results presented in figure 9 indicate that the water retention capacity of both forms of the ionomer is roughly the same from 0% relative humidity to 50% where they start to deviate. At around 60% relative humidity the curves become significantly different. At relative humidity greater than 60%, the hydroxide form of the ionomer will be able to hold more water than the chloride form. We conclude then, that the hydroxide form of the ionomer is more suitable for the zinc-air battery in terms of water retention. Our goal is to retain as much water in the ionomer as possible since increased water retention will bring numerous benefits such as improved ionic conductivity and toughness. Lastly, figure 9 can be used as a tool for calculating the water content of the ionomer at any relative humidity the zinc-air battery will operate in. All that is needed to be known is the dry mass of the ionomer in the battery. This information will certainly be useful for designing a battery cell that will need to operate at various relative humidity.

5.1.4 Swelling Ratio Conclusions

The results presented in the swelling ratio section have similar conclusions to that of the water retention capacity results. For one, the swelling ratio plots presented previously can be used to estimate the diameter and thickness swelling of an ionomer if the dehydrated dimensions and relative humidity are known. This will be particularly useful for battery cell design since the battery cell will need to account for the expansion or contraction of the

polymer membrane in a zinc-air battery when the relative humidity of the environment changes.

Additionally, it can be seen that the shape of the curves in the swelling ratio plots are very similar to those in the water retention capacity plots. This makes sense because the polymer is expected to expand as it absorbs more water. We can see that diameter and thickness expansion is greatest when the relative humidity is highest and lowest when the relative humidity is lowest. The data indicates that lateral expansion is similar for both forms of the ionomer throughout the relative humidity range. However, the hydroxide form of the ionomer clearly had a greater thickness swelling ratio than did the chloride form of the ionomer for a large band of relative humidity. We saw from the water retention capacity data that the hydroxide form of the ionomer can store more water at relative humidity greater than 60%. This excess water storage is reflected in the greater thickness swelling ratio that the hydroxide form has. Furthermore, the data indicates that the hydroxide form of the ionomer has a greater tendency to expand in its thickness than it does in its diameter. We concluded then, that the chloride form of the ionomer would be more desirable for the zinc-air battery since less expansion is desirable. However, the chloride form of the ionomer is not compatible with the zinc-air battery. Therefore, the excess expansion of the hydroxide form of the ionomer will be another challenge in battery cell design.

5.1.5 Pore Size and Presence of Pin Holes Conclusions

The pore density of the ionomer could not be determined precisely. However, based on the data presented, it was concluded that the average pore would have a diameter smaller than 32.6nm. Further investigation of the pore

size and pore distribution would require more advanced techniques and equipment. It is recommended that a mercury intrusion technique coupled with higher magnification SEM be used to gather more precise information regarding the porosity of the ionomer. It is important to know the porosity of an ionomer since oxygen diffusion through the polymer membrane can pose a serious problem for long term battery life. A zinc-air battery can be chemically shorted out if oxygen is allowed to reach the anode. Oxygen will react with zinc to produce zinc oxide directly on the surface of the anode. Zinc oxide is a discharge product of the zinc-anode when the battery cell is being drained and ideally, the zinc oxide is converted back into metallic zinc when the battery cell is recharged. However allowing oxygen to reach the zinc anode directly will defeat the purpose of an electrochemical cell. Thus minimizing oxygen transport through the ionomer by controlling its porosity will be a key design challenge.

5.1.6 Glass Transition Temperature Conclusions

The glass transition temperature of the ionomer is suspected to be around 344°C. However, it also believed that the degradation temperature of the ionomer is very close to this temperature as well. Because degradation was observed during testing, it cannot be concluded with certainty that 344°C is the glass transition temperature of ionomer. Further study would be required to find the glass transition temperature with more confidence in the results. As far as operation within a zinc-air battery goes, it can be concluded that the ionomer would operate at a temperature below its glass transition temperature. This is an indication that the polymer will be in a more brittle like state and could present challenges in manufacturing.

5.1.7 Ionic Conductivity vs Free Salt Content Conclusions

It was concluded that doping the polymer membranes with free salt improved its room temperature ionic conductivity. Furthermore, the ideal salt content range was determined to be 40%-60% by molar amount. This salt content range offers the highest ionic conductivity while preventing the membranes from tearing do to handling. The toughness of the ionomer will be an important design parameter that will need to be considered when manufacturing zinc-air batteries. A polymer membrane that tears too easily could make manufacturing overly difficult. However, operating at a salt content above 60% could still be a feasible solution for improving the ionic conductivity of the ionomer if needed.

5.1.8 Oxygen Concentration and Diffusivity Conclusions

Testing in 0.1M KOH showed that the concentration of oxygen in the ionomer was very close to the concentration of oxygen in the aqueous system, namely 0.1M KOH. Additionally, it was shown that the diffusivity of oxygen in the ionomer was about 4 times less than the diffusivity of oxygen in the aqueous electrolyte. It can be concluded from this experiment that oxygen will in fact be able to reach the zinc anode in a zinc-air battery due to diffusion. Furthermore, the diffusivity and concentration of oxygen within the ionomer could be partly related to its porosity and micro-structure. Ideally, it would be preferred that the concentration and diffusivity of oxygen in the ionomer were non-existent so that the zinc anode does not become oxidized directly by molecular oxygen. However, this is not the case; the thickness of the ionomer will play a significant role in the design of a zinc-air battery cell since it was shown that the concentration and diffusivity of oxygen were non-negligible. A thin ionomer might

offer optimum battery performance but may also significantly reduce the lifetime of the zinc anode due to direct oxidation. On the contrary, using a thicker ionomer might help increase the zinc anode lifetime, but at the cost of battery cell performance. There is no doubt that the electrolyte membrane thickness will play a key role in battery cell design while posing some serious challenges. To leave on a positive note however, it should be emphasized that the methodology described in this work can serve as a useful tool for characterizing the ionomer in future research if modifications can be made to reduce the concentration and diffusivity of oxygen within it.

5.2 Future Work

5.2.1 Optimization of Chemical Reactions

The work described in this document has numerous leads for future research. One important aspect that deserves much attention is the optimization of the chloromethylation and quaternization reaction. It was shown that the product of both reactions was only able to hit about half of the theoretical values. There is no doubt that ionomer properties could be improved, and even fine tuned, if these two reactions can be optimized. Improving the product conversion percentages would be directly beneficial to a zinc-air battery cell. In addition, one could also investigate other suitable tertiary amines for the quaternization reaction. It would be interesting to see how the properties of the ionomer would change as a function of the tertiary amine used.

5.2.2 Future Porosity Study

The porosity of the ionomer was not determined precisely in this work. Although an upper bound was placed on the maximum pore size, it would still be beneficial to investigate the porosity and microstructure of the ionomer more

deeply. A mercury intrusion technique could be used to further gain knowledge about the porosity of the ionomer. High magnification SEM images or imaging with an Atomic Force Microscope could also prove to be useful. Establishing a method of measuring porosity with consistent results will allow a researcher to investigate if the porosity of the ionomer can be manipulated. Perhaps different casting techniques and membrane preparation procedures will yield different porosities in the ionomer. The morphology of the ionomer can also be studied with X-ray florescence. This micro-analytical technique can be used to investigate if any crystallinity is present in the ionomer. Polysulfone is known to be an amorphous polymer, however adding polymer-bound positive charge centers to the ionomer might make the polymer semi-crystalline.

5.2.3 Future Glass Transition Temperature Study

The glass transition temperature of the ionomer was suspected to be around 344°C. However, due to polymer degradation, a glass transition temperature could not be reported with confidence. Further investigation in this subject could lead to better results. One idea is to use plasticizers to lower the glass transition temperature of the ionomer below its degradation temperature so that it can be observed using a DSC technique. Several samples can be prepared with varying plasticizer loading so that a plot of the observed glass transition temperature versus the plasticizer loading can be constructed. This plot can then be extrapolated to the vertical axis to get a better estimate of the glass transition temperature of the ionomer without any plasticizer added. This work can also be advantageous in investigating compatible plasticizers for their use in the zinc-air battery. It was stated before that the brittle state of the ionomer can

pose manufacturing challenges. Using a plasticizer would be an excellent way of attacking any cracking problems.

5.2.4 Future Rotating Disk Electrode Experiments

Lastly, the RDE methodology presented in this document can be used as tool for investigating the diffusivity and concentration of oxygen in future ionomers. As was mentioned earlier, it would be interesting to study how the diffusivity and concentration of oxygen changes when different tertiary amines are used in the quaternization reaction. In addition, the methodology itself can be further improved upon as well since a precise explanation for the observed trend in the data presented in table 10 could not be offered. Future work could revolve around this technique alone and perhaps other electrochemical techniques can be explored as well.

REFERENCES

1.) Wang, Xu, Chenxi Xu, Bernard T. Golding, Masih Sadeghi, Yuancheng Cao, and Keith Scott. "A Novel Phosphoric Acid Loaded Quaternary 1,4-diazabicyclo- [2.2.2]-octane Polysulfone Membrane for Intermediate Temperature Fuel Cells." *International Journal of Hydrogen Energy* 36 (2011): 8550-556. Print.

2.) Wang, Xu, Mingqiang Li, Bernard T. Golding, Masih Sadeghi, Yuancheng Cao, Eileen Hao Yu, and Keith Scott. "A Polytetrafluoroethylene-quaternary 1,4-diazabicyclo-[2.2.2]-octane Polysulfone Composite Membrane for Alkaline Anion Exchange Membrane Fuel Cells." *International Journal of Hydrogen Energy* 36.16 (2011): 10022-0026. Print.

3.) Kumar, Binod, Jitendra Kumar, Robert Leese, Joseph P. Fellner, Stanley J. Rodrigues, and K. M. Abraham. "A Solid-State, Rechargeable, Long Cycle Life Lithium–Air Battery." *Journal of The Electrochemical Society* 157.1 (2010): A50-54. Print.

4.) Gu, Shuang, Rui Cai, Ting Luo, Zhongwei Chen, Minwei Sun, Yan Liu, Gaohong He, and Yushan Yan. "A Soluble and Highly Conductive Ionomer for High-Performance Hydroxide Exchange Membrane Fuel Cells." *Angewandte Chemie International Edition* 48.35 (2009): 6499-502. Print.

5.) X. Lin , L. Wu, Y. Liu , A.L. Ong, S.D. Poynton , J.R. Varcoe , T. Xu, “Alkali resistant and conductive guanidinium-based anion-exchange membranes for alkaline ionomer fuel cells,” *Journal of Power Sources* (2012), doi: 10.1016/j.jpowsour.2012.05.062.

6.) Lu, S., J. Pan, A. Huang, L. Zhuang, and J. Lu. "Alkaline Ionomer Fuel Cells Completely Free from Noble Metal Catalysts." *Proceedings of the National Academy of Sciences* 105.52 (2008): 20611-0614. Print.

7.) Qiao, Jinli, Jing Fu, Rui Lin, Jianxin Ma, and Jianshe Liu. "Alkaline Solid Ionomer Membranes Based on Structurally Modified PVA/PVP with Improved Alkali Stability." *Polymer* 51.21 (2010): 4850-859. Print.

8.) Zeng, Qing Hua, Qing Lin Liu, Ian Broadwell, Ai Mei Zhu, Ying Xiong, and Xing Peng Tu. "Anion Exchange Membranes Based on Quaternized Polystyrene-block-poly(ethylene-ran-butylene)-block-polystyrene for Direct Methanol Alkaline Fuel Cells." *Journal of Membrane Science* 349.1-2 (2010): 237-43. Print.

9.) Abuin, Graciela C., Patrick Nonjola, Esteban A. Franceschini, Federico H. Izraelevitch, Mkhulu K. Mathe, and Horacio R. Corti. "Characterization of an Anionic-exchange Membranes for Direct Methanol Alkaline Fuel Cells." *International Journal of Hydrogen Energy* 35.11 (2010): 5849-854. Print.

10.) Wang, Guigui, Yiming Weng, Deryn Chu, Rongrong Chen, and Dong Xie. "Developing a Polysulfone-based Alkaline Anion Exchange Membrane for Improved Ionic Conductivity." *Journal of Membrane Science* 332.1-2 (2009): 63-68. Print.

11.) Park, Jin-Soo, Gu-Gon Park, Seok-Hee Park, Young-Gi Yoon, Chang Soo Kim, and Won Yong Lee. "Development of Solid-State Alkaline Electrolytes for Solid Alkaline Fuel Cells." *Macromolecular Symposia* 249-250.1 (2007): 174-82. Print.

12.) Mamlouk, M., and K. Scott. "Effect of Anion Functional Groups on the Conductivity and Performance of Anion Exchange Polymer Membrane Fuel Cells." *Journal of Power Sources* 211 (2012): 140-46. Print.

13.) Buruiana, Luminita-Ioana, Ecaterina Avram, Adriana Popa, Valentina Elena Musteata, and Silvia Ioan. "Electrical Conductivity and Optical Properties of a New Quaternized Polysulfone." *Polymer Bulletin* 68.6 (2012): 1641-661. Print.

14.) Pandey, A., A. Goswami, Debasis Sen, S. Mazumder, and Ronald F. Childs. "Formation and Characterization of Highly Crosslinked Anion-exchange Membranes." *Journal of Membrane Science* 217.1-2 (2003): 117-30. Print.

15.) Weber, Adam Z. "Gas-Crossover and Membrane-Pinhole Effects in Polymer-Electrolyte Fuel Cells." *Journal of The Electrochemical Society* 155.6 (2008): B521-531. Print.

16.) Yoshida, Hiroaki, Fumio Takei, and Norio Sawatari. "High Ionic Conducting Polymer with Polysaccharide and Its Applications." *Fujitsu Scientific & Technical Journal* 38.1 (2002): 39-45. Print.

17.) Yan, Xiaomin, Gaohong He, Shuang Gu, Xuemei Wu, Liguang Du, and Yongdon Wang. "Imidazolium-functionalized Polysulfone Hydroxide Exchange Membranes for Potential Applications in Alkaline Membrane Direct Alcohol Fuel Cells." *International Journal of Hydrogen Energy* 37 (2012): 5216-224. Print.

18.) Varcoe, John R. "Investigations of the Ex Situ Ionic Conductivities at 30C of Metal-cation-free Quaternary Ammonium Alkaline Anion-exchange Membranes in Static Atmospheres of Different Relative Humidities." *Physical Chemistry Chemical Physics* 9.12 (2007): 1479-486. Print.

19.) Merle, Geraldine, Seyed Schwan Hosseiny, Matthias Wessling, and Kitty Nijimeijer. "New Cross-linked PVA Based Ionomer Membranes for Alkaline Fuel Cells." *Journal of Membrane Science* 409-410 (2012): 191-99. Print.

20.) Wan, Ying, Katherine AM Creber, Brant Peppley, V. Tam Bui, and Ela Halliop. "New Solid Ionomer Membranes for Alkaline Fuel Cells." *Polymer International* 54.1 (2005): 5-10. Print.

21.) Wang, Junhua, Shenghai Li, and Suobo Zhang. "Novel Hydroxide-Conducting Polyelectrolyte Composed of an Poly(arylene Ether Sulfone) Containing Pendant Quaternary Guanidinium Groups for Alkaline Fuel Cell Applications." *Macromolecules* 43.8 (2010): 3890-896. Print.

22.) Li, Mingtao, Li Yang, Shaohua Fang, and Siming Dong. "Novel Polymeric Ionic Liquid Membranes as Solid Ionomers with High Ionic Conductivity at Moderate Temperature." *Journal of Membrane Science* 366 (2010): 2445-50. Print.

23.) Vinodh, Rajangam, Muthukrishnan Purushothaman, and Dharmalingam Sangeetha. "Novel Quaternized Polysulfone/ZrO2 Composite Membranes for Solid Alkaline Fuel Cell Applications." *International Journal of Hydrogen Energy* 36 (2011): 7291-302. Print.

24.) Cozan, Vasile, Elena Butuc, Ecaterina Avram, and Anton Airinei. "Pendant Functional Group Copolyether Sulfones: III. Modified Copolyether Sulfones with Bisphenolic Copper Chelate." *Applied Organometallic Chemistry* 17.5 (2003): 282-86. Print.

25.) Park, Jin-Soo, Seok-Hee Park, Sung-Dae Yim, Young-Gi Yoon, Won-Yong Lee, and Chang-Soo Kim. "Performance of Solid Alkaline Fuel Cells Employing Anion-exchange Membranes." *Journal of Power Sources* 178.2 (2008): 620-26. Print.

26.) Avram, Ecaterina, Mihai Adrian Brebu, Abraham Warshawsky, and Cornelia Vasile. "Polymers with Pendent Functional Groups. V. Thermooxidative and Thermal Behavior of Chloromethylated Polysulfones." *Polymer Degradation and Stability* 69 (2000): 175-81. Print.

27.) Xie, D., G. Wang, Y. Weng, D. Chu, and Rongrong Chen. "Polysulfone-composed Alkaline Anion Exchange Membrane for Improved Ionic Conductivity." *The Electrochemical Society* 25.13 (2010): 3-14. Print.

28.) Park, J., M. Acar, A. Akthakul, W. Kuhlman, and A. Mayes. "Polysulfone-graft-poly(ethylene Glycol) Graft Copolymers for Surface Modification of Polysulfone Membranes." *Biomaterials* 27.6 (2006): 856-65. Print.

29.) Gu, Shuang, Rui Cai, Ting Luo, Kurt Jensen, Christian Contreras, and Yushan Yan. "Quaternary Phosphonium-Based Polymers as Hydroxide Exchange Membranes." *ChemSusChem* 3.5 (2010): 555-58. Print.

30.) Yan, Xiaomin, Gaohong He, Shuang Gu, Xuemei Wu, Liguang Du, and Haiyan Zhang. "Quaternized Poly(ether Ether Ketone) Hydroxide Exchange Membranes for Fuel Cells." *Journal of Membrane Science* 375 (2011): 204-11. Print.

31.) Fang, J., and P. Shen. "Quaternized Poly(phthalazinon Ether Sulfone Ketone) Membrane for Anion Exchange Membrane Fuel Cells." *Journal of Membrane Science* 285.1-2 (2006): 317-22. Print.

32.) Guo, Tian Yi, Qing Hua Zeng, Chun Hui Zhao, Qing Lin Liu, Ai Mei Zhu, and Ian Broadwell. "Quaternized Polyepichlorohydrin/PTFE Composite Anion Exchange Membranes for Direct Methanol Alkaline Fuel Cells." *Journal of Membrane Science* 371.1-2 (2011): 268-75. Print.

33.) Zhao CH, et al., “Self-crosslinked anion exchange membranes by bromination of benzylmethyl-containing poly(sulfone)s for direct methanol fuel cells”, International Journal of Hydrogen Energy (2012), doi:10.1016/j.ijhydene.2012.04.163

34.) Agrawal, R. C., and G. P. Pandey. "Solid Ionomers: Materials Designing and All-solid-state Battery Applications: An Overview." *Journal of Physics D: Applied Physics* 41.22 (2008): 223001. Print.

35.) Wang, Junhua, Zhuo Zhao, Feixiang Gong, Shenghai Li, and Suobo Zhang. "Synthesis of Soluble Poly(arylene Ether Sulfone) Ionomers with Pendant Quaternary Ammonium Groups for Anion Exchange Membranes." *Macromolecules* 42 (2009): 871110122630016-717. Print.

36.) Yang, Yunsong, Zhiqing Shi, and Steven Holdcroft. "Synthesis of Sulfonated Polysulfone--PVDF Copolymers: Enhancement of Proton Conductivity in Low Ion Exchange Capacity Membranes." *Macromolecules* 37.5 (2004): 1678-681. Print.

37.) Hao, Jihua, Wentong Wang, Puchen Yang, and Qingshuang Zhao. "The Preparation of Quaternized Polysulfone Membrane for Low Pressure Reverse Osmosis." *Desalination* 83.1-3 (1991): 361-71. Print.

38.) Lisa, G., Ecaterina Avram, G. Paduraru, Marinela Irimia, Natalia Hurduc, and N. Aelenei. "Thermal Behaviour of Polystyrene, Polysulfone and Their Substituted Derivatives." *Polymer Degradation and Stability* 82.1 (2003): 73-79. Print.

39.) Hibbs, Michael R., Michael A. Hickner, Todd M. Alam, Sarah K. McIntyre, Cy H. Fujimoto, and Chris J. Cornelius. "Transport Properties of Hydroxide and Proton Conducting Membranes." *Chemistry of Materials* 20.7 (2008): 2566-573. Print.

40.) Maitra, M., K. Verma, M. Sinha, R. Kumar, T. Middya, S. Tarafdar, P. Sen, S. Bandyopadhyay, and U. De. "DSC Characterization of Ion Beam Modifications in Ion Conducting PEO–salt Polymers." *Nuclear Instruments and Methods in Physics Research Section B: Beam Interactions with Materials and Atoms* 244.1 (2006): 239-42. Print.

41.) Karan, N., D. Pradhan, R. Thomas, B. Natesan, and R. Katiyar. "Solid Ionomers Based on Polyethylene Oxide and Lithium Trifluoro-Methane Sulfonate (PEO–LiCF3SO3): Ionic Conductivity and Dielectric Relaxation." *Solid State Ionics* 179.19-20 (2008): 689-96. Print.

42.) "Thermal Properties of Polymers." *Thermal Properties of Polymers*. Case Western Reserve University and Kent State University, n.d. Web. 26 Oct. 2012. <http://plc.cwru.edu/tutorial/enhanced/files/polymers/therm/therm.htm>.

43.) Mani, T., and J. Stevens. "Transparent and Adhesive Ionomer for Smart Windows: Synthesis, Characterization and Ionic Conductivity Measurements." *Polymer* 33.4 (1992): 834-37. Print.

44.) BekkTech LLC. *BekkTech's Procedures For Performing In-Plane Membrane Conductivity Testing*. Loveland: BekkTech LLC, 2008. Print.

45.) Luo, Yanting, Juchen Guo, Chunsheng Wang, and Deryn Chu. "Fuel Cell Durability Enhancement by Crosslinking Alkaline Anion Exchange Membrane Electrolyte." *Electrochemistry Communications* 16 (2012): 65-68. Print.

46.) BekkTech LLC. *General Information on Membrane Conductivity*. Loveland: BekkTech LLC, 2008. Print.

47.) BekkTech LLC. *In Plane Conductivity Testing*. Loveland: BekkTech LLC, 2008. Print.

48.) BekkTech LLC. *In-Plane Conductivity vs. Through Plane Conductivity Measurements*. Loveland: BekkTech LLC. Print.

49.) Clericuzio, M., W. O. Parker Jr, M. Soprani, and M. Andrei. "Ionic Diffusivity and Conductivity of Plasticized Ionomers: PMFG-NMR and Complex Impedance Studies." *Solid State Ionics* 82.3-4 (1995): 179-92. Print.

50.) Cooper, Kevin. "Through-thickness Membrane Conductivity Measurement for HTM Program: Issues and Approach." 2006. TS 1. Scribner Associates, Inc., n.p.

51.) Li, Xuguang, Gang Liu, and Branko N. Popov. "Activity and Stability of Non-precious Metal Catalysts for Oxygen Reduction in Acid and Alkaline Electrolytes." *Journal of Power Sources* 195.19 (2010): 6373-378. Print.

52.) Vega, Jose A., and William E. Mustain. "Effect of CO2, HCO3− and CO3−2 on Oxygen Reduction in Anion Exchange Membrane Fuel Cells." *Electrochimica Acta* 55.5 (2010): 1638-644. Print.

53.) Wu, Jiajia, Dun Zhang, Yi Wang, and Yi Wan. "Manganese Oxide–graphene Composite as an Efficient Catalyst for 4-electron Reduction of Oxygen in Alkaline Media." *Electrochimica Acta* 75 (2012): 305-10. Print.

54.) Lawson, Del R., Lisa D. Whiteley, Charles R. Martin, Marilyn N. Szentirmay, and Jie I. Song. "Oxygen Reduction at Nafion Film-Coated Platinum Electrodes: Transport and Kinetics." *Journal of The Electrochemical Society* 135.9 (1988): 2247-253. Print.

55.) Miyatake, Kenji, Takuya Omata, Donald A. Tryk, Hiroyuki Uchida, and Masahiro Watanabe. "Oxygen Reduction at the Pt/Carbon Black-Polyimide Ionomer Interface." *The Journal of Physical Chemistry C* 113.18 (2009): 7772-778. Print

56.) Okada, Tatsuhiro, Yuusuke Ayato, Jorgen Dale, Makoto Yuasa, Isao Sekine, and Odd A. Asbjornsen. "Oxygen Reduction Kinetics at Platinum Electrodes Covered with Perfluorinated Ionomer in the Presence of Impurity Cations Fe3‘, Ni2‘ and Cu2‘." *Physical Chemistry Chemical Physics* 2 (2000): 3255-261. Print.

57.) Paulus, U.a., T.j. Schmidt, H.a. Gasteiger, and R.j. Behm. "Oxygen Reduction on a High-surface Area Pt/Vulcan Carbon Catalyst: A Thin-film Rotating Ring-disk Electrode Study." *Journal of Electroanalytical Chemistry* 495.2 (2001): 134-45. Print.

58.) Gubbins, Keith E., and Robert D. Walker. "The Solubility and Diffusivity of Oxygen in Electrolytic Solutions." *Journal of The Electrochemical Society* 112.5 (1965): 469-71. Print.

59.) Taurozzi, J., H. Arul, V. Bosak, A. Burban, T. Voice, M. Bruening, and V. Tarabara. "Effect of Filler Incorporation Route on the Properties of Polysulfone–silver Nanocomposite Membranes of Different Porosities." *Journal of Membrane Science* 325.1 (2008): 58-68. Print.

60.) Bowen, W. Richard, Teodora A. Doneva, and H. B. Yin. "Polysulfone—sulfonated Poly(ether Ether) Ketone Blend Membranes: Systematic Synthesis and Characterisation." *Journal of Membrane Science* 181 (2001): 253-63. Print.

61.) *Akshaya Jena and Krishna Gupta.* *Ceramic Bulletin*, Vol. 82, December, 2003, pp. 9401-9406

62.) Avram E, Butuc E, Luca C, Druta I. “Polymers with pendant functional group. 3. Polysulfones containing viologen group.” *J Macromol Sci Pure Appl. Chem*. 1997; A34:1701–14.

63.) Warshawsky A, Dashe A. “Halomethyl octyl ethers: convenient halomethylation reagents.” *J Polym Sci Part A Polym Chem* 1985; 23:1839–41.

64.) Komkova EN, Stamatialis DF, Strathmann H, Wessling M. “Anion-exchange membranes containing diamines: preparation and stability in alkaline solutions.” *J Membr Sci* 2004; 244:25–34.

65.) Xiong Y, Liu QL, Zeng QH. “Quaternized cardo polyetherketone anion exchange membrane for direct methanol alkaline fuel cells.” *J Power Sources* 2009; 193:541e6.

66.) Harrison, W. L.; Wang, F.; Mecham, J. B.; Bhanu, V. A.; Hill, M.; Kim, Y. S.; McGrath, J. E. *J. Polym. Sci., Part A: Polym. Chem.* 2003, 41, 2264.

67.) Pan, Jing, Yan Li, Lin Zhuang, and Juntao Lu. "Self-crosslinked Alkaline Ionomer Exceptionally Stable at 90C." *Chemical Communications* 46 (2010): 8597-599. Print.

68.) Gray F M, McCallum J R and Vincent C A 1986 *Solid State Ion*. 18–19 282

69.) Pandey G P, Hashmi S A and Agrawal R C 2008 *Solid State Ion*. 179 543

70.) Appetecchi G B, Croce F, Doutzenberg G, Mastragostino M, Ronci F, Scrosati B, Soavi F, Zanelli A, Alessandrini F and Prosini P P 1998 *J. Electrochem. Soc*. 145 4126

71.) Prosini P P, Passerini S, Vellone R and Smyrl W H 1998 *J. Power Sources* 75 73

72.) Capiglia C, Yang J, Imanishi N, Hirano A, Takeda Y and Yamamoto O 2000 *Solid State Ion*. 154–155 7

73.) Y. Sone, P. Ekdunge, D. Simonsson, *Journal of the Electrochemical Society*, 143 (1996) 1254-1259.

74.) Qiao JL, Hamaya T, Okada T. New highly proton-conducting membrane poly (vinylpyrrolidone)(PVP) modified poly(vinyl alcohol)/2-acrylamido-2-methyl-1-propanesulfonic acid (PVAePAMPS) for low temperature direct methanol fuel cells (DMFCs). *Polymer* 2005; 46:10809e16.

75.) P. Krishnan, J.-S. Kim, C.-S. Kim, *J. Membr. Sci*. 2006, 279, 220.

76.) R. F. Silva, M. De Francesco and A. Pozio, *J. Power Sources*, 2004, 134, 18–26.

77.) R. F. Silva, M. De Francesco and A. Pozio, *Electrochim. Acta*, 2004, 49, 3211–3219.

78.) Mokrini A and Acosta LJ*, Polymer* 42:8817 (2001).

79.) J.-S. Park, G.-G. Park, S.-H. Park,Y.-G.Yoon, C.-S. Kim,W.-Y. Lee, *Macromol. Symp*. 249/250 (2007) 174–182.

80.) Fujimoto, C. H.; Hickner, M. A.; Cornelius, C. J.; Loy, D. A. *Macromolecules* 2005, 38, 5010.

81.) X. Tongwen, Y. Weihua, *Journal of Membrane Science*, 190 (2001) 159-166.

82.) Z. Zhang, L. Wu, T. Xu, Journal of Membrane Science, 373 (2011) 160-166.

83.) "Standard Test Method for Assignment of the Glass Transition Temperatures by Differential Scanning Calorimetry - E1356." *American Society for Testing and Materials* (2008): 1-4. Print.

84.) Linden, David, and Thomas B. Reddy. "Chapter 38: Metal/Air Batteries." *Handbook of Batteries*. 3rd ed. New York: McGraw-Hill, 2002. N. Print.

85.) Linden, David, and Thomas B. Reddy. "Chapter 13: Zinc/Air Batteries - Button Configuration." *Handbook of Batteries*. 3rd ed. New York: McGraw-Hill, 2002. N. Print.

86.) Beattie, S. D., D. M. Manolescu, and S. L. Blair. "High-Capacity Lithium–Air Cathodes." *Journal of The Electrochemical Society* 156.1 (2009): A44-47. Print.

87.) Yuasa, Masayoshi, Masatoshi Nishida, Tetsuya Kida, Noboru Yamazoe, and Kengo Shimanoe. "Bi-Functional Oxygen Electrodes Using LaMnO3/LaNiO3 for Rechargeable Metal-Air Batteries." *Journal of The Electrochemical Society* 158.5 (2011): A605-610. Print.

88.) Atkins, P. W., and Paula Julio. De. "Chapter 8: Consequences of Equilibrium." *Elements of Physical Chemistry.* 4th ed. Oxford: Oxford UP, 2005. N. Print.

89.) A. K. Jena and K. M. Gupta, Journal of Power Sources, 80 (1999), 46.

90.) Vibhor Gupta and A. K. Jena, Advances in Filtration and Separation Technology, American Filtration & Separation Society, 13b (1999), 833.

91.) Bard, Allen J., and Larry R. Faulkner. "Chapter 9: Methods Involving Forced Convection - Hydrodynamic Methods." *Electrochemical Methods: Fundamentals and Applications*. 2nd ed. New York: Wiley, 2004. N. Print.

92.) Bard, Allen J., and Larry R. Faulkner. "Chapter 14:Electroactive Layers and Modified Electrodes." *Electrochemical Methods: Fundamentals and Applications*. 2nd ed. New York: Wiley, 2004. N. Print

93.) Wells, A. F. *Models in Structural Inorganic Chemistry,*. Oxford: Clarendon P., 1970. Pg 548. Print.

94.) Atkins, P. W., and Paula Julio. De. "Chapter 15: Metallic, Ionic, and Covalent Solids." *Elements of Physical Chemistry.* 4th ed. Oxford: Oxford UP, 2005. N. pg 401. Print.

95.) Atkins, P. W., and Paula Julio. De. "Chapter 14: The Chemical Bond." *Elements of Physical Chemistry.* 4th ed. Oxford: Oxford UP, 2005. N. Print.

96.) LeMay, H. Eugene, Jr., and Bruce E. Bursten. "Chapter 16: Acid-Base Equilibria." *Chemistry: The Central Science.* By Theodore L. Brown. 10th ed. Upper Saddle River, NJ: Pearson Prentice Hall, 2006. N. Print.

97.) "Udel Polysulfone Specifications." Boedeker Plastics : Udel Polysulfone Datasheet. Boedeker Plastics, 2012. Web. 04 June 2012. <http://www.boedeker.com/udel_p.htm>.